3

Actuation mechanisms for microfluidic biomedical devices

A. REZK, J. FRIEND and
L. YEO, RMIT University, Australia

DOI: 10.1533/9780857097040.1.100

Abstract: The dominance of surface and viscous forces at small scales, in particular, render the actuation and manipulation of fluids and particles in microfluidic systems a significant challenge, especially if integration into a portable handheld platform is desired, for example, in miniaturized devices for point-of-care diagnostics and biosensing. We provide a summary of the main actuation techniques that underpin a broad spectrum of microfluidic operations, and, in particular, briefly overview the role of electric and acoustic fields for this purpose. The former are currently mechanisms of choice that are already widely used, whereas the latter, especially surface acoustic waves, comprise an emerging technique that has gained considerable attention of late.

Key words: fluid and particle manipulation, microfluidics, mechanical and non-mechanical actuation, electrokinetics, surface acoustic waves (SAW).

3.1 Introduction

Actuating and manipulating fluids and particles at microscale dimensions poses a considerable challenge, primarily due to the surface area to volume ratio as the characteristic system dimension is reduced, which reflects the increasing dominance of surface and viscous forces in retarding fluid flow. This is captured by the characteristically small Reynolds numbers ($\mathrm{Re} \equiv \rho UL/\mu \lesssim 1$) in microfluidic systems, wherein ρ and μ are the density and viscosity of the fluid, and U and L are the characteristic velocity and length scales, respectively. Laminarity of the flow is also inherent in these low Re systems, thereby highlighting further challenges with regards to fluid mixing, especially in diffusion-limited systems.

To date, external syringe pumps have been widely utilized to induce flow and mixing in microfluidic systems. Although these are precise and reliable, they are fairly large and hence confined to laboratory benchtops, thereby proving difficult to integrate with other operations on the microfluidic device comprising a miniaturized handheld platform for portable

operations, for example, for use at the point of need (Yeo *et al.*, 2011). This is further complicated by the inlet and outlet tubing and ancillary connections required for fluid transfer between the pump and the chip, which requires careful handling by a skilled user, therefore making their use considerably challenging for adoption by patients, for example, in diagnostic testing. The majority of medical testing also involves molecular and bioparticle manipulation, which require additional microfluidic capability for fast and sensitive preconcentration, sorting and detection.

In this chapter, we summarize the various mechanisms for microfluidic actuation within two subcategories: mechanical and non-mechanical actuation mechanisms (Table 3.1). This is followed by a brief overview of two mechanisms, namely electrokinetics and acoustics, which we believe constitute the most promising and practical methods for driving fluid and particle motion in microfluidic devices, as reflected by recent growing interest and popularity in their use.

3.2 Electrokinetics

To date, electrokinetics, which concerns the use of electric fields to manipulate fluid flow, is one of the most preferred and widely used methods for microfluidic actuation. This is because electrodes are cheaply and easily fabricated, and can be integrated without much difficulty in microfluidic devices, and have the ability to provide high electroosmotic flow rates, efficient electrophoretic separation, and precise dielectrophoretic particle positioning. Here, we provide an overview of the basic principles underlying these flows and a brief summary of their use for microfluidic actuation. The reader is referred to a more comprehensive treatise on the subject in Chang and Yeo (2010).

3.2.1 The electric double layer

A channel surface in contact with an electrolyte solution tends to acquire a net charge through various surface-charging mechanisms (Hunter, 1987). Consequently, free ions in the bulk with opposite charge to that on the surface (counter-ions) are attracted to the channel surface, while ions with like charge (co-ions) are repelled. A thin polarized layer rich in counter-ions, known as the Debye double layer, therefore arises adjacent to the channel surface, as depicted in Fig. 3.1a and 3.1b.

The electric potential field φ in the double layer can be described via a solution of Gauss' Law $\nabla^2\varphi = -\rho_e/\varepsilon$ governing charge conservation. For planar systems of symmetrical binary electrolytes, the volume charge density ρ_e can be specified by the Poisson-Boltzmann distribution; in the limit of small

Table 3.1 Summary of the main *mechanical* and *non-mechanical* actuation mechanisms for microfluidic actuation

Mechanical	Principal/Notes	References
Piezoelectric	A diaphragm comprising a piezoelectric disc, or a stack, that deforms when subject to an electric field to induce fluid motion by peristaltic (i.e., sequential contraction and relaxation) action along the length of the channel.	Koch *et al.*, 1998; Schabmueller *et al.*, 2002; Jang *et al.*, 2007; Yang *et al.*, 2008
Pneumatic/ Thermopneumatic	Air is employed to actuate and relax a diaphragm to create a pressure difference that pumps the fluid; often combined with diffusers. Heated and cooled air are used in thermopneumatic versions.	Pol *et al.*, 1990; Jeong and Yang, 2000; Kim *et al.*, 2005; Grover *et al.*, 2006
Rotary/Centrifugal (e.g., rotary gears, Lab-on-a-CD)	Reservoirs, valves and channels are patterned on a compact disc (CD). Fluid actuation within these structures arising from centrifugal forces is achieved upon rotation using a laboratory micromotor. A thermopneumatic addition combines this with heating of the reservoir to allow bidirectional pumping.	Gorkin *et al.*, 2010; Abi-Samra *et al.*, 2011
Shape-memory alloys (SMAs)	SMAs are thin films, and more recently wires, used as valves, pumps, latches and multiplexers due to their ability to exert large strains on soft elastomers such as PDMS under an electric field.	Benard *et al.*, 1998; Xu *et al.*, 2001; Vyawahare *et al.*, 2008
Electromagnetic	Fluid actuation is achieved by applying an oscillating magnetic field with the use of magnetic elements strategically embedded in a soft polymeric structure, resulting in its vibration. This is combined with diffuser and nozzle elements close to the inlets and outlets to achieve net flow direction.	Khoo and Liu, 2000; Al-Halhoulia *et al.*, 2010; Zhou and Amirouche, 2011
Electrostatic	Coulombic attraction force between oppositely charged plates drives the deflection of a soft membrane when an appropriate voltage is applied. The deflected membrane returns to its initial position upon relaxation of the field. The alternating deflection results in a pressure difference that, in turn, pumps the fluid.	Zengerle *et al.*, 1992; Machauf *et al.*, 2005; Bae *et al.*, 2007

Acoustic (e.g., flexural waves, bubble streaming and SAWs)	Flexural Waves: Bulk vibration of a thin piezoelectric film that generates an acoustic field, which, in turn, causes fluid to flow (acoustic streaming). Bubble streaming: Acoustic streaming driven via excitation of bubbles attached at strategic positions on a channel using a piezoelectric transducer. Typically used for fluid mixing and recently for particle sorting and trapping. SAW: MHz order frequency electromechanical surface waves that generate a direct acoustic force on particles or a momentum that generates fluid flow (acoustic streaming) for fluidic actuation and micro/nano particle and biomolecule manipulation.	Moroney *et al.*, 1991; Luginbuhl *et al.*, 1997; Meng *et al.*, 2000 Ahmed *et al.*, 2009a, 2009b; Wang *et al.*, 2012; Hashmia *et al.*, 2012 Friend and Yeo, 2011; Yeo *et al.*, 2011

Non-Mechanical	Principal/Notes	References
Capillary (e.g., pressure and surface tension gradients)	Pressure gradient: Flow induced by a pressure difference across an interface that drives wetting of fluids in channels or in paper-based substrates. Attractive because it offers a passive actuation mechanism without requiring active pumping. Surface tension gradient: Generation of interfacial flow due to chemical (e.g., surfactant) concentration, thermal (thermocapillary), electrical (electrocapillary), or optical (optocapillary) gradients.	Ichikawa *et al.*, 2004; Gervais and Delamarche 2009; Martinez *et al.*, 2010 Darhuber and Troian, 2005; Basu and Gianchandani, 2008
Electrokinetics (e.g., electroosmosis, electrophoresis, dielectrophoresis and electrowetting) – Chang and Yeo (2010)	Electroosmosis: Bulk motion of aqueous solution along a fixed solid boundary due to an external electric field. Electrophoresis: Use of an applied electric field to move charged particles or ions in a stationary fluid. Dielectrophoresis: Motion of dielectric particles suspended in a medium due to the application of a *non-uniform* electric field.	Lazar and Karger, 2002; Takamura *et al.*, 2003; Wang *et al.*, 2009 Wu *et al.*, 2008; Kenyon *et al.*, 2011 Pethig, 2010; Menachery *et al.*, 2010

(*Continued*)

Table 3.1 Continued

Non-Mechanical	Principal/Notes	References
	Electrowetting: Control of the wettability of a drop or film through an applied electric field by the generation of a Maxwell force at the contact line or a Maxwell pressure along the interface (depending on electrode configuration).	Yeo and Chang, 2005; Mugele and Baret, 2005; Wheeler, 2008
Optics (optofluidics) (e.g., laser microfluidic actuation, optical tweezing and, optical chromatography) – Fainman *et al.* (2010)	Laser microfluidic actuation: The momentum carried by incident propagating light gives rise to a radiation pressure at the fluid interface due to the difference in refractive index, resulting in interfacial deformation or even jetting. In addition, localization of the laser beam induces thermocapillary forces leading to fluid flow (see also *Capillary* entry).	Grigoriev, 2005; Baroud *et al.*, 2007; Delville *et al.*, 2009; Dixit *et al.*, 2010
	Optical tweezers: Dielectric particles can be trapped and moved due to the optical gradient within the tightly focused laser beam. Alternatively, birefringence can be exploited in which a particle can be rotated in a standard optical trap simply by manipulating the polarization of the light beam.	Grier, 1997; Dholakia *et al.*, 2002; Chiou *et al.*, 2005; Neale *et al.*, 2005
	Optical chromatography: Use of a focused laser beam to trap particles along its axis of propagation, where the beam is positioned against the fluid flow and the particles' trapped location is a balance between fluid drag and optical pressure.	Imasaka, 1998; Hart and Terray, 2003; Hart *et al.*, 2007
Magnetohydrodynamic	Use of a Lorentz force to pump conducting fluids, perpendicular to both the electric and the magnetic field.	Lemoff and Lee, 2000; Jang and Lee 2000; Bau *et al.*, 2001; Eijel *et al.*, 2003
Microbubbles	Generated either electrochemically (e.g., via electrolysis) or thermally (e.g., cavitation). The bubble oscillation is used to drive pumping in microchannels, often by pushing on diaphragms.	Suzuki and Yoneyama, 2002; Yoshimi *et al.*, 2004; Kabata and Suzuki, 2005; Yin and Prosperetti, 2005

surface potentials $\varphi_s << RT/zF \sim 25.7$ mV (298 K), linearization of the resultant Poisson equation together with boundary conditions prescribed by the surface potential $\varphi = \varphi_s = \lambda_D E_s$ ($y = 0$) and a potential and electric field $E = -d\varphi/dy$ that decays away from the surface to the bulk ($y \to \infty$) permit an approximate analytical solution in the form

$$\varphi = \varphi_s e^{-y/\lambda_D}, \qquad [3.1]$$

where

$$\lambda_D = \sqrt{\frac{\varepsilon RT}{2F^2 z^2 C_\infty}} \qquad [3.2]$$

is the Debye screening length or double layer thickness. The above is known as the *Debye–Hückel approximation* (Debye and Hückel, 1923), wherein y is the coordinate normal to the surface, ε the permittivity, R the molar gas constant, T the absolute temperature, z' the ionic valency, F the Faraday constant and C_∞ the bulk ion concentration. We note the inverse relationship between the Debye length and the ion concentration (and hence conductivity) in Equation [3.2]: strong electrolytes lead to thin double layers (~0.1–10 nm), whereas weaker electrolytes give rise to thicker double layers (~10 nm–1 μm).

The Debye–Hückel approximation, which assumes that the counter-ions are mobile point charges distributed by rapid and random thermal motion in the *diffuse* double layer, nevertheless fails to account for hydration or solvation effects due to the finite ion size. These effects were later taken into account by allowing for a *Stern* layer comprising hydrated counter-ions that are bound by water molecules, whose local screening effect permits their adsorption onto the surface (Fig. 3.1c) (Stern, 1924). A slip plane therefore must exist between the rigid and stationary Stern layer and the mobile diffuse layer, along which the potential, more specifically known as the zeta potential ζ, can be experimentally measured (in contrast to the difficulty in characterizing the actual potential on the surface). For weak to moderate electrolytes, in keeping with the small potential limit in the Debye–Hückel approximation, $\zeta \sim \lambda_D E_s \sim \lambda_D \sigma_s/\varepsilon$.

Electrokinetic phenomena therefore arise as a consequence of slippage of the diffuse double layer over the charged surface upon the application of an applied electric field to generate bulk flow (*electroosmosis* in the case of stationary charged surfaces) or particle motion (*electrophoresis* in the case of a stationary medium), or an applied external force to produce an electric potential (*streaming potential* in the case of flow over a stationary surface or *sedimentation potential* in the case of charged particles moving in

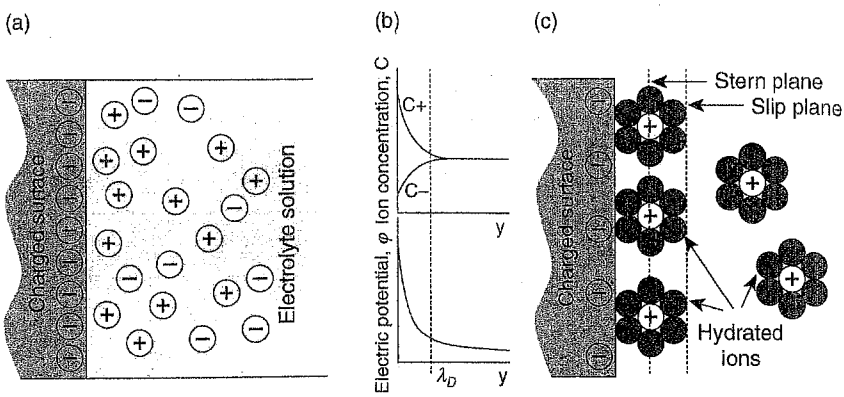

3.1 (a) Schematic depiction of, and (b) concentration profile (top) and electric potential variation (bottom) in the Debye double layer of thickness λ_D that arises as a consequence of an electrolyte solution in contact with charged surface, showing the enrichment in counter-ions and depletion in co-ions. (c) Stern layer that comprises hydrated counter-ions bound by water molecules.

a stationary medium). Given their relevance to microfluidic actuation, we briefly highlight the first two cases in the discussion to follow.

3.2.2 Electroosmosis

Electroosmotic slip

In its most general case, electroosmosis comprises the bulk motion of electrolyte that arises when a tangential electric field is applied across the *equilibrium* double layer that forms when the electrolyte is in contact with a solid boundary that acquires surface charge as a consequence. As depicted in Fig. 3.2, counter-ions in the diffuse layer are attracted to the electrode with opposite polarity, their net charge giving rise to a Maxwell (Lorentz) force $\rho_e E$ and hence momentum transfer on the liquid, which drives an electrokinetic slip at the slip plane. This slip can be derived from a balance between the hydrodynamic viscous and Maxwell stresses, assuming that the double layer is sufficiently thin compared to the channel radius/width such that the flow is unidirectional along the channel and that the pressure gradient only arises as a consequence of the tangential gradient in the normal surface field. Details of the derivation can be found in Chang and Yeo (2010); here, it suffices to quote the result, known as the *Smoluchowski slip velocity*:

$$u_s = -\frac{\varepsilon \zeta E_x}{\mu}, \qquad [3.3]$$

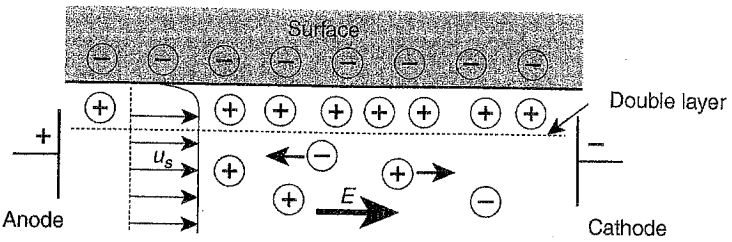

3.2 Counter-ions within the diffuse double layer are attracted towards the electrode with the opposite polarity upon application of a tangential electric field, giving rise to a net Maxwell force and hence bulk motion of the fluid known as electroosmosis. Given the double layer is thin relative to most microchannel dimensions, the flow velocity profile is essentially flat across the channel.

where E_x is the applied tangential field and μ is the viscosity. Typically, ζ ~10–100 mV and hence slip velocities up to around 1 mm/s can be generated with fields of approximately 100 V/cm.

Electroosmotic pumping

The velocity therefore increases from its zero value (i.e., no-slip) at the channel wall to the maximum value given in Equation [3.3] at the slip plane. Consequently, the slip drags the rest of the liquid in the channel along, giving rise to bulk electroosmotic flow. Given the asymptotically small Debye length, the bulk flow can be considered to arise from slip at the channel walls, and hence the velocity profile is essentially flat across the channel. This plug flow is convenient and particularly advantageous over pressure-driven flow from many perspectives, especially for microfluidic applications, since it minimizes hydrodynamic dispersion that leads to sample band broadening. Moreover, the independence of the slip velocity on the channel dimension then suggests that the volumetric flow rate, which is proportional to the channel cross-sectional area, scales as the square of the characteristic channel dimension H^2. This is a considerable advantage over the H^4 scaling of the volumetric flow rate arising from pressure-driven flows, which sharply diminishes with miniaturization of the channel dimension as H decreases. Together with the benefits of on-chip electrode integration – therefore removing the need for cumbersome fluid transfer from large mechanical or syringe pumps onto the microfluidic device, the elimination of mechanically moving parts, the ease of changing the flow direction upon reversal of the electrode polarity and the constant pulse-free fluid motion – electroosmotic pumps thus constitute a very attractive mechanism for microfluidic actuation.

It can further be shown from simple scaling arguments that a channel dimension H close to λ_D optimizes the power efficiency of the electroosmotic

pump (Chang and Yeo, 2010) – in larger channels, power is wasted in the large electroneutral bulk region outside the double layer where there is no net momentum transfer due to the absence of net charge, whereas in smaller channels, the flow is suppressed by increased viscous dissipation. As such, and given that the volumetric flow rate scales with cross-sectional area, it is expedient to employ a parallel bundle of thin channels (e.g., nanopores) whose dimensions are comparable to the double layer thickness – an example being that in packed capillaries or porous silica monoliths (Chen *et al.*, 2005; Wang *et al.*, 2006). For cylindrical pore geometries, and neglecting the tortuosity of the pore networks, the maximum pressure that can be developed in such pumps, taking into account the hydrodynamic load that imposes a back pressure within a channel, can be expressed by

$$\Delta p_{\max} = \frac{8\mu Q_{eo}}{\left(A_p R_p^2 / L_p\right) + \left(A_l R_l^2 / L_l\right)}, \qquad [3.4]$$

where $Q_{eo} = u_s A_p = n\pi R_p^2 u_s$ is the electroosmotic flow rate of the pump comprising n cylindrical pores of radius R_p and length L_p, i.e., the maximum flow rate when there is no pressure-driven flow ($\Delta p = 0$), and $A_l = \pi R_l^2$ the effective cross-sectional area of the hydrodynamic load section with radius R_l and length L_l, whose flow rate is specified by the Hagen-Poiseuille equation:

$$Q = \frac{A_l R_l^2}{8\mu} \frac{\Delta p_{\max}}{L_l}. \qquad [3.5]$$

Substituting Equation [3.4] into Equation [3.5],

$$Q = Q_{eo}\left(1 - \frac{\Delta p}{\Delta p_{\max}}\right), \qquad [3.6]$$

indicating the linear relationship between the back pressure and flow rate, and from which the efficiency of the pump can be obtained:

$$\eta = \frac{Q}{Q_{eo}} = 1 - \frac{\Delta p}{\Delta p_{\max}}. \qquad [3.7]$$

The pump becomes more efficient therefore as $\Delta p_{\max}$ increases, which, from Equation [3.4], can be obtained by reducing R_p/R_l such that Q approaches

Q_{eo}. This is however constrained, since decreasing R_p below λ_D results in overlapping double layers and hence diminishing slip velocities. The pump operation is therefore optimal when $R_p \sim \lambda_D$, as suggested above, noting from Equation [3.4] that Q_{eo}, and hence Q, can be compensated by increasing the applied field strength, although this, on the other hand, is limited by undesirable effects of bubble generation as a consequence of the increased current, which can cause blockage of the channel and whose large capillary pressures could cancel out any increase in the flow rate.

The theory above, nevertheless, breaks down for nanochannels when the channel dimension becomes comparable to the Debye length, such that an electroneutral ohmic region in the bulk no longer exists and the entire channel consists of a polarized region due to double layer overlap. In addition, entrance, resistive, pore neck charge storage, and electroviscous effects may also become important in these cases (Chang and Yeo, 2010). There are several analytical models as well as molecular simulations dedicated to nanochannel electroosmosis (see, for example, Petsev (2010) and Qiao and Aluru (2003)); we refer the reader to these, as the subject is beyond the scope of the present overview.

Electroosmotic mixing

Given the irrotationality of the electric field, the similarity between the hydrodynamic streamlines and the electric field – i.e., both velocity and electric fields are governed by the same divergence-free conditions – renders the electroosmotic flow an irrotational potential flow (hence the flat velocity profiles observed in Fig. 3.2) in the absence of an externally applied pressure gradient (Chang and Yeo, 2010). An unfortunate consequence of this result, which is quite unexpected for microfluidic flows where viscous stresses are usually dominant, is the absence of flow vortices to induce mixing in the microfluidic device, which, although advantageous in minimizing sample dispersion as discussed earlier, can be problematic given the typically low biomolecular diffusivities that result in long reaction times in transport-limited cases. Various strategies have therefore been adopted to increase mixing efficiency in electroosmotic flows. For example, it is possible to revoke the field and streamline similarity by generating a back pressure gradient in the channel through the introduction of surface charge, or bulk pH or electrolyte concentration (and hence ζ-potential) gradients along the channel (Ajdari, 1995; Herr *et al.*, 2000; Minerick *et al.*, 2002). Alternatively, interfacial instabilities can be introduced in the case of two co-flowing electrolytes with differences in their conductivities (Lin *et al.*, 2004; Pan *et al.*, 2007), as illustrated in Fig. 3.3, although the electric fields required to drive such transverse electrokinetic instabilities are often fairly large.

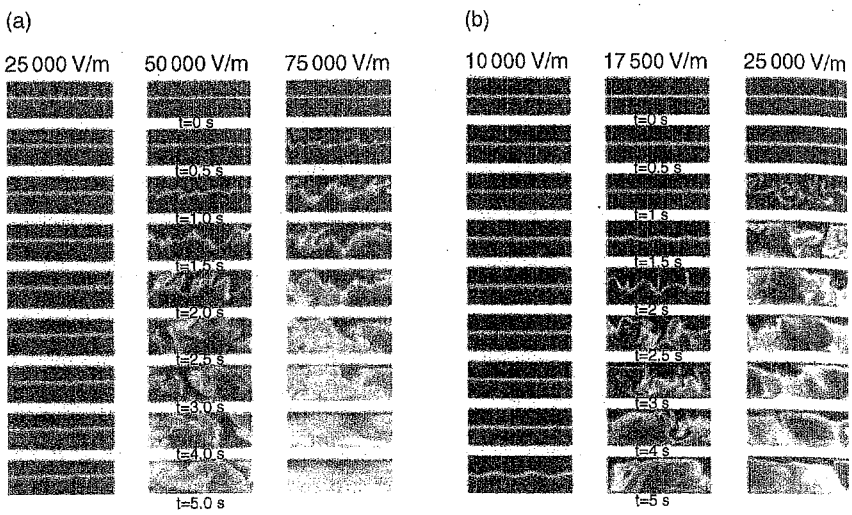

3.3 Transient electrokinetic instability driven by the gradient in the conductivity of two co-flowing electrolyte solutions under an applied longitudinal electric field. (a) Experimental results and (b) numerical simulation. (*Source*: Reprinted with permission from Lin *et al.* (2004). Copyright 2004, American Institute of Physics.)

3.2.3 Electrophoresis

Electrophoresis refers to the application of electric fields to move charged particles or ions in a stationary fluid. Two asymptotic limits for the particle size a can be considered (Chang and Yeo, 2010). In the small particle size limit (Fig. 3.4a), i.e., $a << \lambda_D$, the particle can be assumed to be a point charge and hence double layer screening effects can be neglected. In this case, the presence of the point charge does not influence and hence distort the field lines, and simply translates under electromigration effects in the absence of electrokinetic slip in the double layer around the particle. A balance between the Coulomb force exerted by the point charge q and the viscous drag force then leads to the Hückel equation for the electrophoretic mobility of the particle:

$$v_{ep} = \frac{2\varepsilon\zeta}{3\mu}, \qquad [3.8]$$

which is related to the electrophoretic velocity through $u_{ep} = v_{ep}E$.

In the large particle size limit (Fig. 3.4b), i.e., $a >> \lambda_D$, the double layer screens the external field, and hence the Maxwell force only acts in the double layer to drive an electrokinetic slip flow and not on the particle itself.

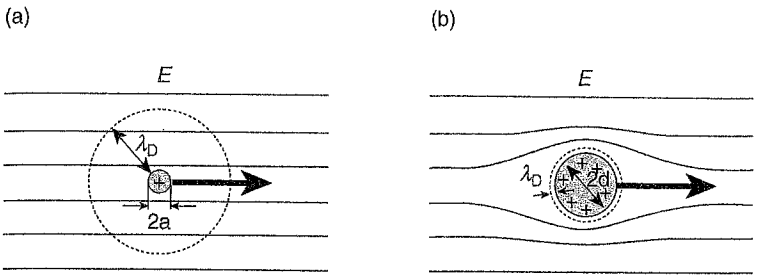

3.4 (a) The electric field lines around a particle remain undistorted around a charged particle if its size *a* is small compared to the Debye double layer thickness ($a << \lambda_D$). (b) On the other hand, the double layer screens the external field when the particle size is large compared to the double layer thickness ($a >> \lambda_D$).

In this case, the Smoluchowski slip velocity in Equation [3.3] can be used along the particle surface such that the electrophoretic velocity has the same dependency as the electroosmotic slip velocity but with opposite sign:

$$u_s = \frac{\varepsilon \zeta E_x}{\mu}. \qquad [3.9]$$

The discrimination in the electrophoretic mobility and hence migration velocity based on charge (more specifically, the surface charge density and hence the ζ-potential) in Equations [3.8] and [3.9] provides the underlying basis for electrophoretic separation technology. We note, however, the absence of the dependence on particle size or shape (although the former is implicit in the ζ-potential in the point charge theory). More common, however, is the use of gels or polymer (i.e., gel electrophoresis), which provides a medium that acts as a molecular sieve to facilitate steric and reptation effects, thus permitting size-based discrimination (i.e., smaller molecules migrate more quickly in the gel compared to larger molecules with the same electrophoretic mobility under the same electric field). More recently, a powerful technique has been proposed as an alternative to gel electrophoresis, in which the ends of polyelectrolyte molecules are tagged with a large uncharged monodispersed protein or polymer that exerts a large drag on the molecule whilst leaving its net charge intact. This technique, known as end-labelled free-solution electrophoresis (Meagher *et al.*, 2005), has been demonstrated as a fast and efficient method for the separation of gene fragments in DNA sequencing. Other methods for multiplex DNA sequencing using capillary array electrophoresis in microfluidic platforms (Paegel *et al.*, 2002), as well as electrophoretic detection of DNA sequence variations in microfluidic devices, have also been proposed – for the latter see, for example, the

work on single nucleotide polymorphism detection using restriction fragment length polymorphism (Footz *et al.*, 2004) and single-strand conformation polymorphism (Szántai and Guttman, 2006). The reader is also referred to the review by Wu *et al.* (2008) and Yeo *et al.* (2011).

We note that the buffer solution also moves due to electroosmosis, and hence the electroosmotic velocity must be taken into account. Defining an electroosmotic mobility $v_{eo} = u_s/E$, the apparent mobility and hence the apparent velocity of the charged particle moving through the buffer solution under combined electrophoresis and electroosmosis is simply the sum of the electrophoretic and electroosmotic mobilities. When the charged particles have the same polarity as that of the ions in the buffer solution, the apparent mobility therefore exceeds the electrophoretic mobility, whereas the converse is true if the charged species has the opposite polarity to the ions in solution. Interestingly then, the charged particles can be trapped when the electrophoretic and electroosmotic mobilities are equal, which can be exploited to reduce the length required for electrophoretic separation.

To date, several extensions to the above electrophoretic theories have been proposed with more sophisticated theories to account for electroviscous effects – including that for non-spherical (Chen and Koch, 1996) and porous particles (Natraj and Chen, 2002), tangential surface conduction (Camp and Capitano, 2005), counter-ion condensation (Chang and Yeo, 2010), as well as conducting Stern layer and convective currents effects (Shubin *et al.*, 1993).

3.2.4 AC electrokinetics

The use of DC electric fields is not without inherent disadvantages. High DC field intensities can sustain large currents that cause molecular and cellular degradation, and particle aggregation, as well as bubble and ion contamination generation. These problems can, however, be circumvented with the use of high frequency (>10 kHz) AC fields. The polarization mechanism and hence flow dynamics associated with AC electrokinetics are, however, fundamentally different from its DC or low frequency AC counterpart. Above frequencies associated with time scales that are below the double layer charge relaxation time scale $\lambda_D^2/D = \varepsilon/\sigma$, wherein D is the ionic diffusivity and σ the conductivity, there is insufficient time to polarize the double layer. As such, AC electrokinetics utilizes the electric field itself to induce polarization on the electrode surface in place of polarization due to the natural surface charges on the channel surface, as in DC electrokinetics (Chang and Yeo, 2010). Correspondingly, the induced polarization is non-uniform, given the double layer is no longer in equilibrium; as a result, the ζ-potential is now field-dependent, and thus it can be seen, for example, from the slip velocity given by Equation [3.3], that AC electrokinetic phenomena are

non-linear. Moreover, at these high frequencies, electrochemical reactions at the electrodes are usually absent at the RMS voltages typically employed, and hence problems associated with bubble and ion generation are non-existent. Further, the AC current is localized in the double layer, therefore minimizing penetration and thus damage in molecular and cellular structures. Below, we provide only a very brief summary of this subject in the context of AC electroosmosis; for a more in-depth discourse on non-linear and non-equilibrium electrokinetics, the reader may wish to consult the text by Chang and Yeo (2010). It is worth noting that it is possible to drive similar field-induced double layer polarization using DC fields (alternatively known as induced-charge electrokinetic phenomena (Squires and Quake, 2005), also discussed further in Chang and Yeo (2010)).

The simplest case of AC electroosmotic flow occurs due to capacitive charging over symmetric coplanar electrodes, as illustrated in Fig. 3.5; it is also possible that AC electroosmotic flows can be generated due to Faradaic charging (Lastochkin *et al.*, 2004; Ng *et al.*, 2009), although we will refrain from discussing this mechanism here. In one half of the AC cycle, ions in the bulk are driven by the field towards electrodes of opposite polarity to form a double layer whose total charge balances that on the electrodes. In the next half cycle, the electrode polarity reverses and so does that of the double layer on each electrode. In both cases, however, an outward tangential Maxwell force arises, which does not reverse in direction upon reversal of the field. This therefore gives rise to a net non-zero time-average Maxwell stress and hence an electroosmotic slip to result in a pair of recirculating vortices with length scales comparable to the electrode dimension. This symmetric vortex pair, however, cancels and hence no net flow is produced. In order to create a net global flow, it is therefore necessary to break the vortex symmetry with the use of asymmetric electrodes or an asymmetric field (e.g., a travelling wave) (Ajdari, 2000; Brown *et al.*, 2000; Ramos *et al.*,

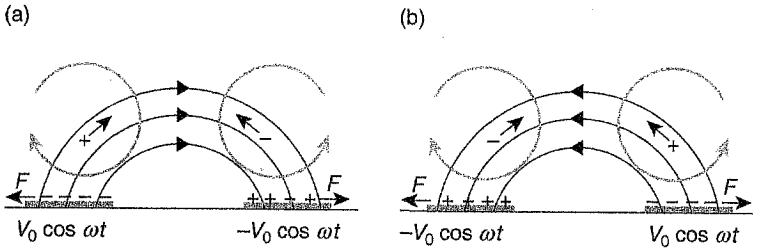

3.5 Schematic of AC electroosmotic flow on symmetric coplanar electrodes that is due to the capacitive charging mechanism. (a) and (b) show the electric field directions, the resultant time-averaged Maxwell force, and the corresponding flow profiles in successive AC half-cycles. (*Source*: After Ben and Chang (2005).)

2003); practical devices also include an upper surface to suppress the back flow associated with the larger vortex. In fact, the most efficient flow can therefore be produced with maximum asymmetry through an orthogonal (T) electrode design given the near singular field at the tip of the vertical section of the 'T' (Lastochkin *et al.*, 2004). First derived by González *et al.* (2000), the time-averaged AC electroosmotic slip on the electrode can be shown to assume the form

$$u_s = -\frac{\varepsilon_l}{4\mu}\nabla_s \left|\Phi \mp \frac{V_0}{2}\right|^2, \qquad [3.10]$$

where Φ is the potential in the bulk immediately adjacent to the double layer and $|V_0|$ the RMS amplitude of the applied voltage signal; ∇_s is a surface gradient operator across each electrode. It is then apparent from this, together with a charge balance across the double layer,

$$\sigma\frac{\partial\varphi}{\partial n} = i\omega C\left(\Phi - \frac{V_0}{2}\right) \qquad [3.11]$$

(where ω is the applied AC frequency, C the total capacitance in the double layer, and n the coordinate normal to the electrode surface) that the slip velocity reaches a maximum at an optimum frequency ω_0 associated with the RC or double layer charging time (R being the electrolyte resistance) $D/\lambda_D d$, where d is the electrode separation. Away from this optimum frequency, the slip velocity decays monotonically to zero. At low frequencies $\omega \to 0$, the double layer is completely polarized and completely screens the field such that the electrode resembles a perfect insulator; consequently, the potential drop occurs mainly across the double layer. At high frequencies $\omega \to \infty$, there is insufficient time to charge the double layer, and hence the electrode resembles a constant potential surface (i.e., a perfect conductor) and the potential drop occurs mainly across the bulk (Chang and Yeo, 2010).

Squires and Bazant (2004) later extended the analysis of AC electroosmotic flows to allow for charging on ideally polarizable surfaces other than electrodes. In particular, they examined a conducting cylinder (e.g., a metal wire) immersed in an electrolyte, which when subjected to a uniform field, attracted the normal field lines, thus facilitating normal field penetration into the double layer and giving rise to an electroosmotic slip (Fig. 3.6). Again, the time-averaged slip velocity exhibits a maximum due to complete screening in the low frequency limit and incomplete charging in the high frequency limit. In any case, the resulting flow is quadrupolar as shown in

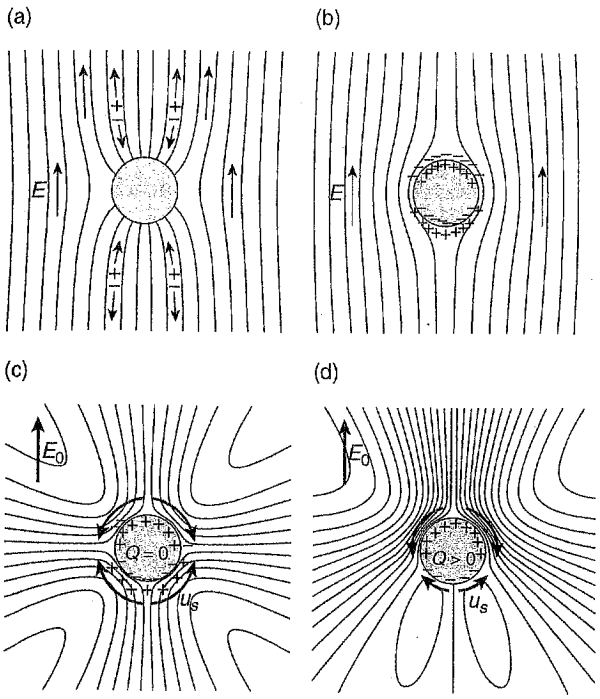

3.6 Double layer charging mechanisms of a polarizable conducting cylinder immersed in an electrolyte solution. Field lines (a) before and (b) after charging of the double layer. (c) Resulting electroosmotic flow streamlines, and (d) the corresponding streamlines obtained if the net charge on the cylinder surface is non-zero. (*Source*: Reprinted with permission from Squires and Bazant (2004). Copyright 2004, American Physical Society.)

Fig. 3.6c, wherein fluid is drawn along the field lines at the poles and ejected radially at the equator.

In addition to micropumping applications, the planar converging stagnation flow associated with the recirculating vortex pair in AC electroosmosis above symmetric coplanar electrodes has also been exploited for linear particle assembly (Ben and Chang, 2005). A similar system was later used to convect single DNA molecules in a bulk suspension and immobilize them onto the electrode surface for subsequent stretching (Lin *et al.*, 2005). Long-range convective trapping of DNA has also been demonstrated using the T-electrode design – the horizontal section of the 'T' being used to sweep particles in the bulk toward the vertical section of the 'T' which then funnels the concentrated particles into a conical region (Du *et al.*, 2008). Whilst such long-range convective mechanisms are not extremely effective at local trapping, since flow conservation renders a true stagnation point impossible, it is possible to combine the AC electroosmotic flow with short-range forces to

provide enhanced particle localization. Dielectrophoresis is one such short-range mechanism, which we shall discuss next.

3.2.5 Dielectrophoresis

Upon application of an electric field, a dielectric particle suspended in a dielectric medium acquires an interfacial charge due to the discontinuity in the permittivity across the phases. The interfacial polarization, however, is dependent on the orientation of the field due to the alignment of the individual dipoles within the particle and medium with the field, which can collectively be described by a single particle dipole that produces an effective dipole moment. For a spherical particle of radius a under an external AC field $\mathbf{E}$, upon solving for the potential of the particle and the medium through an expansion in spherical harmonics, this takes the form (Chang and Yeo, 2010)

$$\mathbf{p} = 3\varepsilon_m f_{\mathrm{CM}} V \mathbf{E}, \qquad [3.12]$$

where

$$f_{\mathrm{CM}} = \frac{\widetilde{\varepsilon_p} - \widetilde{\varepsilon_m}}{\widetilde{\varepsilon_p} + 2\widetilde{\varepsilon_m}} \qquad [3.13]$$

is the Clausius–Mossotti factor that describes the polarizability of the particle. In the above, V is the particle volume and

$$\widetilde{\varepsilon_i} = \varepsilon_i - i\frac{\sigma_i}{\omega} \qquad [3.14]$$

is a complex permittivity in which the subscripts p and m denote particle and medium properties, respectively. When subject to an applied AC electric field with constant phase, this induced effective particle dipole then results in a time-averaged force on the particle, which reads (Green and Morgan, 1999):

$$\langle \mathbf{F} \rangle = \frac{1}{T}\int_0^T (\mathbf{p}\cdot\nabla)\tilde{\mathbf{E}}\,\mathrm{d}t = \pi\varepsilon_m a^3 \,\mathrm{Re}\left[f_{\mathrm{CM}}\right]\nabla|\mathbf{E}|^2, \qquad [3.15]$$

where T denotes the period of AC forcing.

We note that the force is short range, depending on the particle dimension cubed as well as the electric field gradient. This non-uniform field is

necessary since the net interfacial charge on both ends of the particle are of opposite polarities but equal magnitudes; the force therefore cancels out in a uniform field since there is no effective dipole moment. The resulting particle motion that arises from this interaction between the non-uniform field with the induced dipole moment is therefore known as dielectrophoresis (DEP).

The versatility of DEP manipulation arises from the reversal in the polarizability specified by the real part of the Clausius–Mossotti factor $\mathrm{Re}[f_{CM}]$ about a crossover frequency

$$\omega_c = \frac{1}{2\pi}\sqrt{\frac{(\sigma_m - \sigma_p)(\sigma_m + 2\sigma_p)}{(\varepsilon_p - \varepsilon_m)(\varepsilon_p + \varepsilon_m)}}. \qquad [3.16]$$

For frequencies at which $\mathrm{Re}[f_{CM}] > 0$, particles are thus drawn toward regions of high field intensity (positive DEP), whereas for frequencies at which $\mathrm{Re}[f_{CM}] < 0$, particles are drawn toward regions of low field intensity (negative DEP). The dependence of f_{CM} on the particle and medium conductivities and permittivities also allows the design of a DEP sorter that endows one particle species with a positive DEP force and another with a negative DEP force through judicious choice of a specific applied frequency (Gagnon and Chang, 2005). Multiple species, for example, can also be sorted by different DEP mobilities, which can be estimated from a balance between the DEP force in Equation [3.15] and the Stokes drag on the particle:

$$v_{DEP} = \frac{\varepsilon_m a^2 \,\mathrm{Re}[f_{CM}]}{6\mu}. \qquad [3.17]$$

An integrated multiplex continuous flow microfluidic platform for filtering debris and for sorting and trapping of colloidal beads or pathogens at a rate of 100 particles/s is shown in Fig. 3.7 (Cheng *et al.*, 2007). Whilst this sorting rate is still two orders of magnitude smaller than conventional flow cytometry, the technology offers the possibility for carrying out cell sorting and identification with costs and portability that are not afforded by laboratory-based cell sorters.

Consequently, DEP has emerged as a powerful tool for size-based discrimination for microfluidic detection and sorting. Numerous applications for DEP cell (blood cells, stem cells, neuronal cells, pathogens) sorting and characterization, pathogen (bacterial and viral) detection, and DNA, protein and chromosomal manipulation are summarized in the excellent review by Pethig (2010). Given the emergence of bead-based assays to enhance

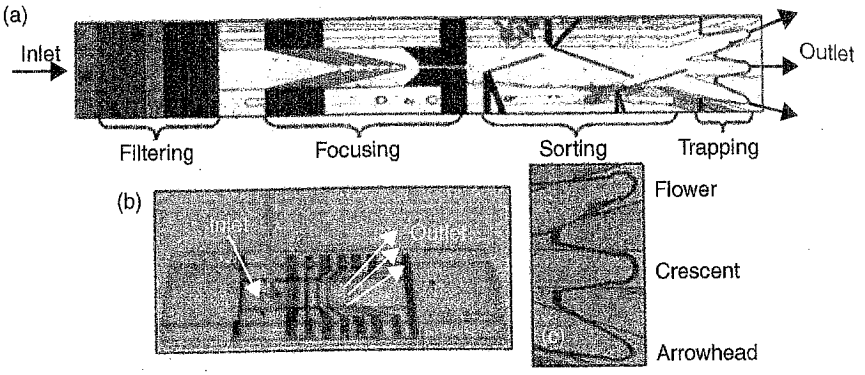

3.7 Bioparticle filtering, focusing, sorting, trapping and detection using an integrated dielectrophoretic chip. (a) Image of the setup comprising different bioparticle manipulation stages. (b) Image showing the electrodes fabricated on two glass slides, giving rise to three-dimensional effects. (c) A top view of the three different trapping electrode configuration, comprising a flower – multiple curved electrode, crescent – a semicircle electrode, and an arrowhead – a pointed electrode. (*Source*: Reprinted with permission from Cheng *et al.* (2007). Copyright 2007, American Institute of Physics.)

detection, for example, in DNA hybridization and sequencing assays (Yeo *et al.*, 2011), we anticipate DEP will play a major role in facilitating rapid and precise bead identification and sorting in microfluidic devices. Already, it has been shown that DNA concentration and the hybridized DNA conformation has a strong influence on the crossover frequency and the effective bead hydrodynamic radius (Gagnon *et al.*, 2009). This was exploited for trapping silica nanocolloids functionalized with oligonucleotides complementary to specific target DNA sequences for rapid microfluidic DNA identification in under 10 min. Beyond diagnostics and biosensing applications, DEP has also been used for isolating and positioning single cells in a similar manner to optical tweezers but with the advantage of design simplicity and significantly lower costs, primarily given that an expensive and complex laser is not required (Menachery *et al.*, 2011).

3.3 Acoustics

Despite its many advantages, electrokinetic actuation technology is hampered by the necessity for external ancillary equipment such as signal generators and amplifiers, which render complete miniaturization and integration with the microfluidic chip difficult. This is further compounded by the limitation of electrolyte solutions, which may be prohibitive in certain cases, and the requirement for high voltages in some other cases. An

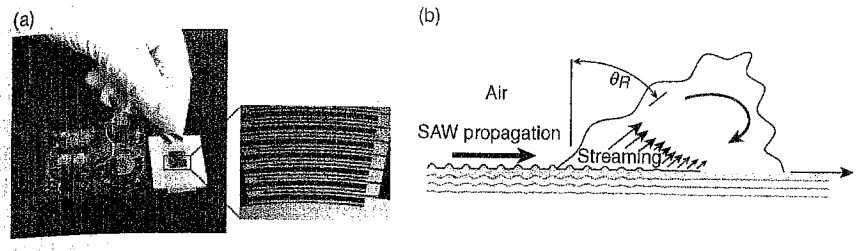

3.8 (a) A typical SAW device comprising a piezoelectric substrate on which IDT electrodes are patterned (as shown in the enlarged inset) and a portable battery-operated electronic circuit and power supply. (b) Schematic depiction of the Eckart streaming generated when energy leaks into a drop at the Rayleigh angle θ_R when it is irradiated by SAWs propagating along the underlying substrate.

alternative mechanism that has demonstrated significant promise is the use of acoustic fields to drive microfluidic actuation, which has the ability to generate relatively large throughput and high pressures. Whilst fairly low voltages are required, this is however compromised by the large sizes of the piezoelectric transducers often required to generate bulk ultrasonic manipulation that do not facilitate easy integration and miniaturization. Further, the large stresses that arise from the vibration, with frequencies typically of the order of 10–100 kHz and up to 1 MHz, and, in many cases, the accompanying cavitation that ensues, inflict considerable biomolecular and cellular damage.

These limitations, however, can be circumvented with a technology that has attracted considerable traction of late – the use of SAWs (Yeo and Friend, 2009; Friend and Yeo, 2011). Since the piezoelectric substrate required could comprise the microfluidic chip itself and as the interdigital transducer (IDT) electrodes required to generate the SAW can be integrated on the substrate, there is no need for the large transducers typically used in conventional ultrasonic microfluidics. Moreover, it has been shown that the ability to access high (MHz order and above) frequencies significantly limits the amount of molecular damage caused. One further advantage is the typically low powers ($\leq$1 W) required to drive fluid and particle actuation with SAWs, even to the point of fluid atomization, thereby allowing the entire operation to be driven using a portable driver circuit powered by camera batteries, which, together with the chip-scale substrate (Fig. 3.8a), potentially allows for complete miniaturization and integration into a truly handheld and portable microfluidic device (Yeo and Friend, 2009). Here, we briefly discuss the basic principles underlying acoustic fluid and particle actuation, and review developments in the field to date, particularly focusing on the SAW technology.

3.3.1 Basic principles of acoustic fluid and particle manipulation

A sound wave is the result of pressure or velocity oscillations that propagate through a compressible medium, and can be generated through bulk or surface vibration of solid materials. A convenient way to produce such vibration, especially at small scales in microfluidic systems, is with the use of oscillating electric fields by exploiting the electromechanical coupling afforded by piezoelectric transducers or substrates. There are primarily two broad strategies employed for acoustic particle and fluid actuation, which we describe next.

The first, generally known as *acoustophoresis*, exploits standing acoustic waves set up in a resonator configuration to spatially trap and move cells. The fundamental basis of the particle localization at pressure nodes/antinodes of the standing wave, and hence the ability to carry out particle separation, arises from a competition between the dominant forces acting on the particle (assuming that sedimentation and buoyancy forces are negligible), namely, the primary acoustic radiation force

$$F_a = -kE_aV_p\phi(\beta,\rho)\sin(2kx), \qquad [3.18]$$

assuming a one-dimensional planar standing wave, and the drag force

$$F_d = -6\pi\mu a \qquad [3.19]$$

acting on the particle of dimension a and volume V_p, in which x is the distance from a pressure node along the wave propagation axis. In the above, $k = 2\pi f/c_l$ is the wave number, with f denoting the applied frequency and c_l the sound speed in the fluid medium, $E_a = p_0^2\beta_l/4 = p_0^2/4K_l = p_0^2/4\rho_l c_l^2$ the acoustic energy density of the standing wave, with p_0 being the pressure amplitude of the standing wave, β_l the liquid compressibility, K_l the bulk modulus, ρ_l the liquid density, and

$$\phi = \frac{5\rho_p - 2\rho_l}{2\rho_p + \rho_l} - \frac{\beta_p}{\beta_l}, \qquad [3.20]$$

is an acoustic contrast factor in which ρ_p and β_p are the particle density and compressibility, respectively. Particles therefore aggregate at the pressure nodes for $\phi > 0$ and at the antinodes for $\phi < 0$.

The second exploits the fluid flow that results as the acoustic wave propagates through a fluid, known as *acoustic streaming* (Friend and Yeo, 2011).

Different acoustic streaming phenomena are observed to occur over a variety of length scales imposed by the system geometry. In a thin boundary layer of fluid immediately adjacent to the vibrating surface with a characteristic thickness defined by the viscous penetration depth $(2\nu/\omega)^{1/2}$, strong viscous dissipation of the acoustic wave gives rise to flow known as *Schlichting streaming* (Schlichting, 1932), which is vortical in nature due to the no-slip condition at the oscillating solid boundary; ν is the kinematic viscosity and ω the frequency. At the edge of the boundary layer (also known as the Stokes layer) over a length scale on the order of the sound wavelength in the liquid λ_L (which, in turn, is related to the excitation frequency), a steady irrotational drift flow, known as *Rayleigh streaming*, occurs as a consequence of the periodic recirculation in the boundary layer (Rayleigh, 1884; Manor *et al.*, 2012). Over longer length scales $>> \lambda_L$, the viscous dissipation of the acoustic radiation due to absorption in the fluid, whose pressure and velocity fluctuations gives rise to a time-averaged particle displacement and hence steady momentum flux (i.e., Reynolds stress), which is non-zero despite the harmonic oscillation due to the non-linear effects arising from viscous attenuation of the wave (Lighthill, 1978); the resultant flow being known as *Eckart streaming* (Eckart, 1948). It is not uncommon for a combination or all of the various streaming phenomena to exist together in a system, although one particular mechanism typically dominates, contingent on the system geometry. This is reflected in the flow phenomena observed, which can be remarkably distinct depending on the particular streaming mechanism that gives rise to them (Rezk *et al.*, 2012a).

3.3.2 Bulk ultrasonic vibration

The majority of the early work on acoustically-driven microfluidic actuation was focused on the use of bulk ultrasonic transducers. These typically consisted of thin plates or membranes comprising a piezoelectric ceramic along which flexural waves (i.e., asymmetric Lamb waves) were generated, the plate/membrane thickness being a fraction of the wavelength of the flexural wave. For example, Moroney *et al.* (1991) and Meng *et al.* (2000) coated silicon nitride onto a ground plate, followed by the deposition of a thin zinc oxide layer and subsequently the aluminium interdigital electrodes. The bulk vibration that ensued then drove acoustic streaming, which due to the large attenuation length for the 1 MHz order employed, extended over a long range, typically a few centimetres from the membrane (Luginbuhl *et al.*, 1997); as such, the device can also be used for mixing applications (Yaralioglu *et al.*, 2004). Nevertheless, these flexural wave pumps are not as efficient compared to the SAW fluid actuation which we discuss in the next section, with larger powers required, and one to two orders of magnitude

lower in the velocity (typically up to 100 μm/s) that can be produced, even when focusing electrodes are employed (Meng *et al.*, 2000).

In a similar manner, it is also possible to exploit substrate vibration to depin contact lines, and to drive droplet motion in open microfluidic platforms. In the former, a contact line hysteresis condition for a drop subject to vibration was derived in which the depinning was dependent on the vibrational acceleration (Noblin *et al.*, 2004); in other work, the drop could be shown to spread under 1 MHz order piston-like thickness mode vibration of the underlying substrate, which induced a boundary layer streaming flow that endowed an additional surface force at the contact line (Manor *et al.*, 2011). In the latter, a flexurally vibrating beam was employed by Alzuaga *et al.* (2005) on which different modes were excited in order to translate the drop between nodal locations.

Ultrasound-induced bubble oscillation can also be exploited to induce oscillatory flows, particularly useful for micromixing, or to facilitate nucleic acid transfection across cell membranes (i.e., sonoporation), even to the point of cell lysis (Ohl *et al.*, 2006). In these cases, the bubbles are sonicated at resonance (typically kHz order) to induce a strong flow known as *cavitational microstreaming* that arises as the sound energy is dissipated due to the fluid viscosity in a boundary layer surrounding the bubble (Nyborg, 1958). Pumping flows of around several mm/s can be achieved, for example, with multiple bubbles housed in a cavity array, and can be used to drive micromixing (Tovar and Lee 2009) or even cell sorting (Patel *et al.*, 2012). More examples of the use of bubble oscillation in microfluidics can be found in the review by Hashmi *et al.* (2012). Whilst relatively fast flows with reasonable throughput on the order of 100 μL/min and efficient mixing can be generated using bubble-based microfluidic actuators, difficulties associated with generating, trapping and maintaining the stability of bubbles is a common problem that has yet to be adequately resolved, in addition to limitations arising from molecular/cell lysis due to cavitational damage that can be undesirable in bioapplications other than gene transfection.

Much more progress has been observed on the acoustophoretic front, on the other hand, in which ultrasonic standing waves are employed to focus particles onto nodal lines for cell sorting (Harris *et al.*, 2005), colloidal filtering (Hawkes and Coakley, 2001) or particle switching (Manneberg *et al.*, 2009) applications. Particles can also be separated based on size by exploiting the discrepancy in the size scaling between Equations [3.18] and [3.19] and hence the dependence of the particle migration time on the particle dimension (larger particles aggregate more quickly compared to smaller ones); such fractionation is more specifically known as free-flow acoustophoresis when conducted in a continuous flow system with the particles being driven orthogonally to the flow. Other design variations have also been investigated, for example flow splitting (Johnson and Feke, 1995) and frequency

switching (Liu and Lim, 2011). Two vastly different particle species can also be separated given that the acoustic radiation force switches directions between positive and negative contrast factors in Equation [3.20] – a property that was exploited for separating lipids from red blood cells (Petersson *et al.*, 2004). The reader is referred to Laurell *et al.* (2007) for a more detailed discussion on acoustophoresis and its applications.

3.3.3 Surface acoustic waves (SAW)

Nanometre amplitude surface vibrations on a substrate in the form of Rayleigh waves offer an attractive and arguably superior alternative for microfluidic actuation compared to bulk ultrasound. The energy localization of these SAWs on the substrate and their efficient coupling into the fluid allows fluid actuation to be carried out with significantly lower dispersive losses, and hence the power requirement to drive comparable fluid actuation to that generated by bulk acoustics is significantly less, by one to two orders of magnitude, therefore offering the possibility for battery-powered operation, which, together with the chip-scale SAW device in Fig. 3.8a, enables attractive miniaturization possibilities (Yeo and Friend, 2009). Further, the low powers, together with the higher frequencies accessible with the SAWs, 10 MHz and above, have been found to suppress shear or cavitation damage on molecules (Qi *et al.*, 2010), thus making them attractive for bioapplications.

The SAW can be generated on a piezoelectric substrate by applying a sinusoidal electrical signal to IDT electrodes patterned on the substrate, whose finger width d determines the frequency f of the SAW and hence its wavelength λ_{SAW}, i.e., $f = c_s/4d = c_s/\lambda_{SAW}$. As illustrated in Fig. 3.8b, the coupling of acoustic energy into the fluid to drive Eckart streaming (Section 3.3.1) then arises from the diffraction of the SAW front in the presence of the fluid, which leads to leakage of the energy into the fluid at the Rayleigh angle, defined as the ratio between the sound speed of the Rayleigh wave on the substrate c_s to the speed of sound in the fluid c_l, i.e., $\theta_R = \sin^{-1}(c_s/c_l)$. In addition to the recirculation within the fluid, the acoustic radiation pressure also imparts a force at the interface, that together with the momentum transfer to the interface due to Eckart streaming, imparts a body force on the drop whose horizontal component causes it to translate in the direction of the SAW. Similarly, the elliptical retrograde motion of solid elements on the substrate as the SAW traverses underneath the drop also induces Schlichting and Rayleigh streaming, which has been shown to pull out a thin front-running wetting film in the opposite direction to that of the SAW propagation (Manor *et al.*, 2012; Rezk *et al.*, 2012a). In the same way that ultrasonic standing waves and acoustic streaming can be exploited to drive microscale fluid actuation and particle manipulation, we provide a short

discussion of the use of SAWs for this purpose and their associated applications. For a more detailed discussion on SAW microfluidics, see, for example, Friend and Yeo (2011).

SAW particle manipulation

Acoustophoretic manipulation can also be carried out using standing SAWs in a similar manner to bulk ultrasonic standing waves (Section 3.3.2). The standing wave, in the SAW devices, however, arises when diffraction of the SAW from the substrate into the liquid (Fig. 3.8b) generates sound waves in the liquid bulk that reflects off the walls of the microchannel (often fabricated from polydimethylsiloxane (PDMS) and placed on top of the SAW substrate). Depending on the channel dimension and the sound wavelength in the fluid, the particles then aggregate along one or more pressure nodal (or antinodal) lines along the channel. Conventionally, the IDTs are placed perpendicular to the channel and hence flow direction (Shi *et al.*, 2008) to achieve linear focusing and subsequent separation/sorting, for example, by size, compressibility or density (Nam *et al.*, 2012). In addition, the IDTs can also be arranged orthogonally at two lateral sides of a square chamber to obtain two-dimensional patterning (Shi *et al.*, 2009). A discussion on the use of these devices as 'acoustic tweezers' for cell manipulation is given by Lin *et al.* (2012).

In addition, the nodal and hence particle positions can also be shifted along the axis of the standing wave by shifting the relative phase between the input IDT signal (Meng *et al.*, 2011; Orloff *et al.*, 2011). Particle alignment and sorting can also be carried out using IDTs placed at the ends of the channel such that the SAW propagates along the channel axis (Tan *et al.*, 2009a). One advantage of this configuration is the ability to alter between fluid pumping and particle focusing simply by switching the frequency from the fundamental mode to a higher harmonic (Tan *et al.*, 2010).

SAW fluid actuation and manipulation

SAW particle aggregation, trapping, patterning and separation is typically carried out at low input powers, considerably below 1 W, where the SAW displacement amplitude and velocity are relatively small, on the order of 0.1 nm and 0.01 m/s, respectively, such that the streaming is weak in order to avoid dispersion of the particles. At these low powers, other particle patterning phenomena are also observed, for example, those that form on the nodes or antinodes of capillary waves induced on the free surface of drops vibrated by the SAW excitation (Li *et al.*, 2008).

At moderate power levels (approximately up to 1 W), it is possible to dispense and transport drops (Renaudin *et al.*, 2006). For example, sessile drops

can be translated on the substrate when the acoustic radiation pressure and acoustic streaming results are sufficient to impart momentum transfer to the interface to overcome the pinning of the contact line (Brunet *et al.*, 2010). This was shown for a variety of applications in open microfluidic systems such as polymerase chain reactions (Wixforth *et al.*, 2004), bioparticle sampling, collection and concentration (Tan *et al.*, 2007), scaffold cell seeding (Li *et al.*, 2007a), and protein unfolding (Schneider *et al.*, 2007). In addition, SAW droplet manipulation, such as mixing and particle concentration as well as sensing, has also been combined with electrowetting to enhance drop manipulation operations such as drop positioning and splitting (Li *et al.*, 2012).

At these powers, the SAW can also be used to drive strong convective flows both within the drop and in channels. For example, it is possible to break the planar symmetry of the SAW to drive azimuthal recirculation in a drop or a microfluidic chamber to generate a rapid microcentrifugation effect (Li *et al.*, 2007b; Shilton *et al.*, 2008). This was used for example for inducing rapid and chaotic mixing (Shilton *et al.*, 2011) (Fig. 3.9a), which can be used to enhance chemical and biochemical reactions (Kulkarni *et al.*, 2009, 2010), or for particle concentration/separation (Fig. 3.9b). It is also possible to sort two particle species based on size in this microcentrifugation flow by exploiting the discrepancy in the scaling between the acoustic radiation force and the drag force exerted on the particle (Equations [3.18] and [3.20]): from a balance between these two forces, it is then possible to derive a frequency-dependent crossover particle size (which, in certain respects, is an analogue to the dielectrophoretic crossover frequency in Equation [3.15]) below which the drag force dominates to drive smaller particles to the centre of the drop and above which the acoustic force dominates to drive larger particles to the periphery (Fig. 3.9c) (Rogers *et al.*, 2010). Finally, the drop rotation can also be used to spin 100 μm–10 mm thin SU-8 discs on which microfluidic channels and chambers can be patterned, as a miniaturized counterpart to the Lab-on-a-CD (Madou *et al.*, 2006) for centrifugal microfluidic operations; unlike the Lab-on-a-CD, however, the SAW miniaturized Lab-on-a-Disc (miniLOAD) platform does not require a laboratory bench-scale motor, as the SAW can be driven using a portable driver circuit (Fig. 3.8a), therefore constituting a completely handheld microfluidic platform (Fig. 3.10) (Glass *et al.*, 2012).

SAW streaming has been demonstrated for fluid actuation in PDMS channels placed atop the substrate (Masini *et al.*, 2010), in channels ablated into the SAW substrate (Tan *et al.*, 2009a), and even on paper (Rezk *et al.*, 2012b). In addition, it was also shown that the SAW can be used to deflect the interfaces of co-flowing streams for directing emulsion droplets (Franke *et al.*, 2009) and sorting cells (Franke *et al.*, 2010). Whilst the body of earlier work was carried out in open microchannels, which have severe limitations

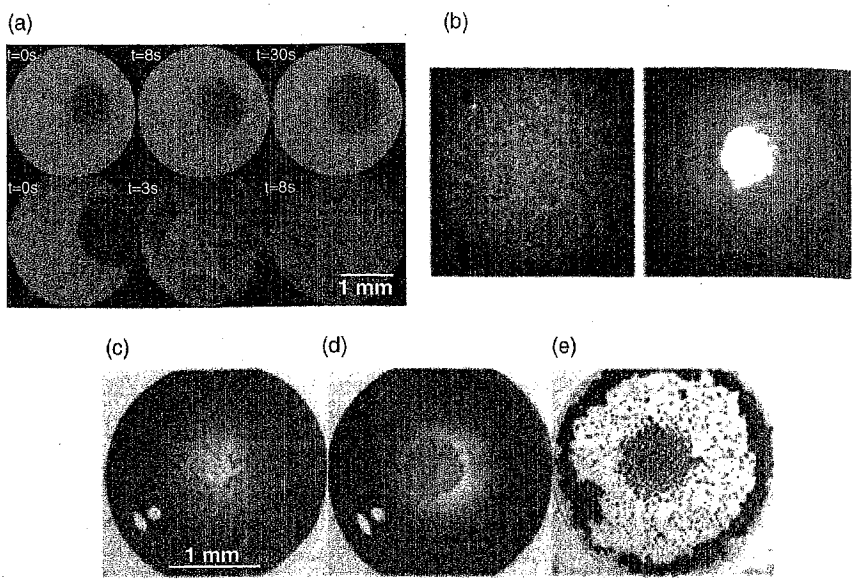

3.9 (a) The images in the top row show mixing of a dye due to pure diffusion without the action of the SAW, whereas the images in the bottom row show effective mixing under chaotic flow conditions driven by the SAW with an input power of ~1 W. (*Source*: After Shilton *et al.* (2011).) (b) Concentration of particles in a 0.5 μL drop via drop rotation induced by acoustic radiation due to the SAW. (*Source*: After Shilton *et al.* (2008).) (c)–(e) Separation of pollen and synthetic particles. (*Source*: After Rogers *et al.* (2010).) (c) Prior to the application of the SAW, the pollen and synthetic particles were suspended homogeneously throughout the entire quiescent drop. (d) After 3 s of applying the SAW, the pollen particles appear to concentrate in the centre of the drop and are hence separated from the synthetic particles, which tend to concentrate along the periphery of the drop. (e) The two species remain separated even after removal of the SAW and when the drop is fully evaporated after 1 min.

due to evaporation and possible contamination, recent work has focused on fluid actuation in a closed PDMS microchannel loop (Schmid *et al.*, 2012) although the efficiency of the pump remained modest as a consequence of the strong absorption of the acoustic energy by the PDMS channel placed atop the SAW substrate. A way to circumvent this limitation was proposed by Langelier *et al.* (2012), in which a glass superstrate housing the microchannel was directly bonded to the SAW substrate using UV epoxy; alternatively, an SU-8 glue layer can also be used (Johanssen *et al.*, 2012). Importantly, it was shown that the SAW is retained at the interface between the substrate and superstrate. This is in contrast to previous uses of a superstrate, first proposed by Hodgson *et al.* (2009), in which a fluid layer between the SAW substrate and the superstrate was employed to couple the

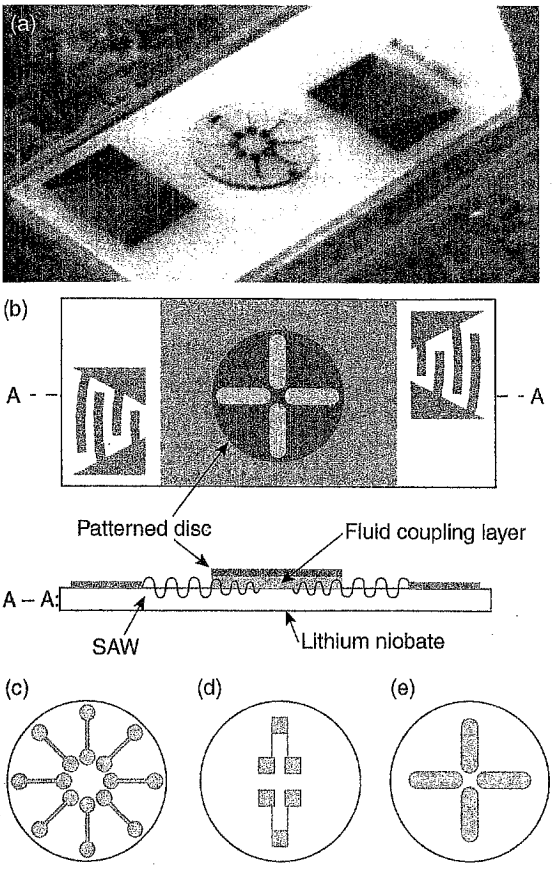

3.10 (a) Image and (b) schematic depiction of the miniLOAD platform comprising a 10 mm diameter SU-8 disc on which microchannels with a variety of designs ((c)–(e)) are fabricated to demonstrate capillary valving, micromixing and particle concentration/separation on a miniaturized centrifugal platform. The disc rotation is driven by coupling an asymmetric pair of SAWs into the fluid underneath the disc. (*Source*: Reprinted with permission from Glass *et al.* (2012). Copyright 2012, Wiley.)

acoustic energy into the latter, resulting in a Lamb wave on the superstrate. Nevertheless, it was shown, that it is possible to achieve similar fluid actuation and particle manipulation on the superstrate through Lamb wave excitation, albeit at a cost of considerably lower efficiency. Regardless, the use of a superstrate remains attractive since the microfluidic operations can be carried out in conventional silicon-based materials, which are considerably cheaper, thus allowing the option of disposability. Bourquin *et al.* (2010) later showed that it was possible to pattern periodic arrays of holes or posts in the superstrate to form a phononic crystal lattice that acted as a bandgap

to drive similar azimuthal recirculation to that discussed for a drop above, or to filter, scatter, reflect or focus the Lamb wave. This was employed for the development of a biosensor platform for the concentration of beads labelled with antibodies onto surface sites for subsequent binding and fluorescent detection (Bourquin *et al.*, 2011).

At higher power, above 1 W, it is possible to drive sufficient interfacial deformation of a film or a drop to extrude fluid jets (Tan *et al.*, 2009b; Bhattacharjee *et al.*, 2011) or to drive atomization (Qi *et al.*, 2008). Given that a monodispersed distribution of 1–10 μm aerosol droplets can be formed in the latter without requiring nozzles or orifices, the latter is particularly useful for pulmonary drug delivery (Qi *et al.*, 2009), especially the next generation of therapeutic agents such as DNA, peptides and proteins, in a miniaturized portable platform for point-of-care therapeutics and personalized medicine. A significant advantage of the SAW pulmonary delivery platform over conventional nebulizers is the ability to preserve the viability of the drug, particularly shear-sensitive molecules such as DNA and peptides. In addition to drug delivery, the SAW atomization platform has been shown to be an efficient ionization source for microfluidic mass spectrometry interfacing (Heron *et al.*, 2010; Ho *et al.*, 2011). The atomization of polymer solutions using the SAW is also a rapid technique for template-free polymer patterning for microarray applications (Alvarez *et al.*, 2008a) as well as for synthesizing 100 nm dimension protein and polymer nanoparticles (Alvarez *et al.*, 2008b; Friend *et al.*, 2008) within which drugs can be encapsulated (Alvarez *et al.*, 2009). This was more recently extended to synthesize nanocapsules of complementary polyelectrolyte layers for DNA encapsulation, as an example of tunable controlled release delivery (Qi *et al.*, 2011).

3.4 Limitations and future trends

Microscale and nanoscale fluid actuation and particle manipulation comprises the underpinning technology which enables a revolutionary field that could potentially provide innovative solutions for chemical and biological applications by performing tasks much faster, cheaper, with considerably less reagent volume, and ideally more easily – tasks that include DNA amplification by polymerase chain reaction, chemical synthesis, proteomics, and point-of-care diagnostics, among others (Robinson and Dittrich, 2013). Yet, the primary limitation that besets this enabling technology is at present posing a severe bottleneck in the development of true integrated and miniaturized devices for these applications: the inability to scale down and incorporate compact and efficient fluid actuation and particle manipulation with the rest of the microfluidic operations on the chip device. Whilst bench-scale capillary pumps and ancillary equipment such as amplifiers, signal generators, lasers, transducers and motors are adequate in driving reasonably

fast and efficient fluid actuation in a microfluidic chip for demonstrative purposes, such large and cumbersome components, and the difficulties of incorporating them on the chip, are impracticable when true portable functionality – the underlying motivation for adopting microfluidics in many applications – is desired.

Beyond miniaturization, another considerable challenge that has yet to be overcome is actuation efficiency. At present, the best fluidic actuation technologies that can be incorporated onto a chip, although not without their own challenges, are not comparable with their macroscopic counterparts in terms of efficiency. Electrokinetic and acoustic pumps, for example, have the ability to generate fast flow rates, but cannot match capillary pumps as far as the pressures that can be generated are concerned. Particle and cell manipulation schemes have sorting efficiencies and throughputs that are well below those achievable with conventional fluorescent activated cell sorting (FACS) technology, often by over two to three orders of magnitude. Further, long term reliability of microfluidic actuation technology has yet to be demonstrated. Another challenge that has yet to be widely addressed is chip automation and control – without which the device would be inoperable by an untrained user, thus defeating the goal of the 'Lab on a Chip' for point-of-care use and rendering the device closer in concept to a 'Chip-in-a-Lab'.

With continued advances in the research and development in microscale fluid actuation, we nevertheless believe that these challenges can be overcome. It is our opinion, however, that the solution may not necessarily lie with a single technology, but rather by combining several complementary technologies such that the limitations of a particular technology may be overcome with the strengths of another. An example of such that has already been demonstrated is the combination of fast, long-range electroosmotic convection and precise, short-range trapping offered by DEP. We anticipate further technology combinations in the future, especially cross-platform technologies such as the integration of acoustofluidics and electrokinetics.

Nanoscale actuation is another exciting area in which we foresee further growth given the promise for nanofluidic platforms (Mukhopadhyay, 2006; Napoli *et al.*, 2010; Piruska *et al.*, 2010), in particular for single molecule manipulation and sensing. Considerable work has been undertaken to date to elucidate mechanisms that govern nanoscale transport (Rauscher and Dietrich, 2008; Schoch *et al.*, 2008; Chang and Yossifon, 2009; Sparreboom *et al.*, 2009; Zhou *et al.*, 2011) and we anticipate their widespread translation into practical technology in the near future. Nanofluidic actuation, nevertheless, faces similar, if not more challenging, hurdles to those encountered by its microfluidic counterpart, most importantly in practical device integration, given the additional complication of dealing with the micro/nano interface.

3.5 References

Abi-Samra, K., Clime, L. Kong, L., Gorkin III, R., Kim, T. H., Cho, Y. K. and Madou, M. (2011) 'Thermo-pneumatic pumping in centrifugal microfluidic' *Microfluid. Nanofluid.*, **11**, 643–652.

Ahmed, D., Mao, X., Juluri, B. K. and Huang, T. J. (2009a) 'A fast microfluidic mixer based on acoustically driven sidewall-trapped microbubble' *Microfluid. Nanofluid.*, **7**, 727–731.

Ahmed, D., Mao, X., Shi, J, Juluria, B. K. and Huang, T. J. (2009b) 'A millisecond micromixer via single-bubble-based acoustic streaming' *Lab Chip*, **9**, 2738–2741.

Ajdari, A. (1995) 'Electro-osmosis on inhomogeneously charged surfaces' *Phys. Rev. Lett.*, **75**, 755–758.

Ajdari, A. (2000) 'Pumping liquids using asymmetric electrode arrays' *Phys. Rev. E*, **61**, R45–R48.

Al-Halhoulia, A. T., Kilanib, M. I. and S. Büttgenb, S. (2010) 'Development of a novel electromagnetic pump for biomedical applications' *Sens. Actuat. A: Phys.*, **162**, 172–176.

Alvarez, M., Friend, J. R. and Yeo, L. Y. (2008a) 'Surface vibration induced spatial ordering of periodic polymer patterns on a substrate' *Langmuir*, **24**, 10629–10632.

Alvarez, M., Friend, J. R. and Yeo, L. Y. (2008b) 'Rapid generation of protein aerosols and nanoparticles via SAW atomisation' *Nanotechnology*, **19**, 455103.

Alvarez, M., Friend, J. R. and Yeo, L. Y. (2009) 'Rapid production of protein loaded biodegradable microparticles using surface acoustic waves' *Biomicrofluidics*, **3**, 014102.

Alzuaga, S., Manceau, J.-F. and Bastien, F. (2005) 'Motion of droplets on solid surface using acoustic radiation pressure' *J. Sound Vib.*, **282**, 151–162.

Bae, B., Han, J., Masel, R. I. and Shannon, M. A. (2007) 'A bidirectional electrostatic microvalve with microsecond switching performance' *J. Microelectromech. Sys.*, **16**, 1461–1471.

Baroud, C. N., Vincent, M. R. S. and Delville, J.-P. (2007) 'An optical toolbox for total control of droplet microfluidics' *Lab Chip*, **7**, 1029–1033.

Basu, A. S. and Gianchandani, Y. B. (2008) 'Virtual microfluidic traps, filters, channels and pumps using Marangoni flows' *J. Micromech. Microeng.*, **18**, 115031.

Bau, H. H., Zhong, J. and Yi, M. (2001), 'A minute magneto hydro dynamic (MHD) mixer' *Sens. Actuat. B: Chem.*, **79**, 205–213.

Ben, Y. and Chang, H. C. (2005) 'Nonlinear electrokinetic devices', in *The MEMS Handbook*, ed. M. Gad-el-Hak (CRC Press, Boca Raton).

Benard, W. L., Kahn, H., Heuer, A. H. and Huff, M. A. (1998) 'Thin-film shape-memory alloy actuated micropumps' *J. Microelectromech. Sys.*, **7**, 245–251.

Bhattacharjee, P. K., McDonnell, A. G., Prabhakar, R., Yeo, L. Y. and Friend, J. R. (2011) 'Extensional flow of low-viscosity fluids in capillary bridges formed by pulsed surface acoustic wave jetting' *N. J. Phys.*, **13**, 023005.

Bourquin, Y., Reboud, J., Wilson, R. and Cooper, J. M. (2010) 'Tuneable surface acoustic waves for fluid and particle manipulations on disposable chips' *Lab Chip*, **10**, 1898–1901.

Bourquin, Y., Reboud, J., Wilson, R., Zhang, Y. and Cooper, J. M. (2011) 'Integrated immunoassay using tuneable surface acoustic waves and lensfree detection' *Lab Chip*, **11**, 2725–2730.

Brown, A. B. D., Smith, C. G. and Rennie, A. R. (2000) 'Pumping of water with ac electric fields applied to asymmetric pairs of microelectrodes' *Phys. Rev. E*, **63**, 016305

Brunet, P., Baudoin, M., Matar, O. B. and Zoueshtiagh, F. (2010) 'Droplets displacement and oscillations induced by ultrasonic surface acoustic waves: a quantitative study' *Phys. Rev. E*, **81**, 036315.

Camp, J. P. and Capitano, A. T. (2005) 'Size-dependent mobile surface charge model of cell electrophoresis' *Biophys. J.*, **113**, 115–122.

Chang, H.-C. and Yossifon, G. (2009) 'Understanding electrokinetics at the nanoscale: a perspective' *Biomicrofluidics*, **3**, 012001.

Chang, H.-C. and Yeo, L. Y. (2010) *Electrokinetically Driven Microfluidics and Nanofluidics* (Cambridge University, New York).

Chen, S. B. and Koch, D. L. (1996) 'Rheology of dilute suspensions of charged fibres' *Phys. Fluids*, **8**, 2792–2807.

Chen, Z., Wang, P. and Chang, H.-C. (2005)' An electro-osmotic micro-pump based on monolithic silica for micro-flow analyses and electro-sprays' *Anal. Bioanal. Chem.*, **382**, 817–824.

Cheng, I.-F., Chang, H.-C., Hou, D. and Chang, H.-C. (2007) 'An integrated dielectrophoretic chip for continuous bioparticle filtering, focusing, sorting, trapping, and detecting' *Biomicrofluidics*, **1**, 021503.

Chiou, P. Y., Ohta, A. T. and Wu, M. C. (2005) 'Massively parallel manipulation of single cells and microparticles using optical images' *Nature*, **436**, 370–372.

Darhuber, A. A. and Troian, S. M. (2005) 'Principles of microfluidic actuation by modulation of surface stresses' *Annu. Rev. Fluid Mech.*, **37**, 425–455.

Debye, P. and Hückel, E. (1923) 'Zut Theorie der Electrolyte. II. Das Grenzgesetz für die elektrishe Leitfähigkeit' *Phys. Z.*, **24**, 305–325.

Delville, J.P., de Saint Vincent, M. R., Schroll, R. D., Chraibi, H., Issenmann, B., Wunenburger, R., Lasseux, D., Zhang, W. W. and Brasselet, E. (2009) 'Laser microfluidics: fluid actuation by light' *J. Opt. A*, **11**, 034015.

Dholakia, K., MacDonald, M. and Spalding, G. (2002) 'Optical tweezers: the next generation' *Phys. World*, **15**, 31–35.

Dixit, S. S., Kim, H., Vasilyev, A., Eid, A. and Faris, G. W. (2010) 'Light driven formation and rupture of droplet bilayers' *Langmuir*, **26**, 6193–6200.

Du, J.-R., Juang, Y.-J., Wu, J.-T. and Wei, H.-H. (2008) 'Long-range and superfast trapping of DNA molecules in an ac electrokinetic funnel' *Biomicrofluidics*, **2**, 044103.

Eckart, C. (1948) 'Vortices and streams caused by sound waves' *Phys. Rev.*, **73**, 68–76.

Eijel, J. C. T., Dalton, C., Hayden, C. J., Burt, J. P. H. and Manz, A. (2003) 'A circular AC magnetohydrodynamic micropump for chromatographic applications' *Sens. Actuat. B:Chem.*, **92**, 215–221.

Fainman, Y., Lee, L., Psaltis, D. and Yang, C. (2010) *Optofluidics: Fundamentals, Devices, and Applications* (McGraw-Hill, New York).

Footz, T., Somerville, M. J., Tomaszewski, R., Elyas, B. and Backhouse. C. J. (2004) 'Integration of combined heteroduplex/restriction fragment length polymorphism analysis on an electrophoresis microchip for the detection of hereditary haemochromatosis' *Analyst*, **129**, 25–31.

Franke, T., Abate, A. R., Weitz, D. A. and Wixforth, A. (2009) 'Surface acoustic wave (SAW) directed droplet flow in microfluidics for PDMS devices' *Lab Chip*, **9**, 2625–2627.

Franke, T., Braunmüller, S., Schmid, L., Wixforth, A. and Weitz, D.A. (2010) 'Surface acoustic wave actuated cell sorting (SAWACS)' *Lab Chip*, **10**, 789–794.

Friend, J. R. and Yeo, L. Y. (2011) 'Microscale acoustofluidics: microfluidics driven via acoustics and ultrasonics' *Rev. Mod. Phys.*, **83**, 647–704.

Friend, J. R., Yeo, L. Y., Arifin, D. R. and Mechler, A. (2008) 'Evaporative self-assembly assisted synthesis of polymer nanoparticles by surface acoustic wave atomization' *Nanotechnology*, **19**, 145301.

Gagnon, Z. and Chang, H.-C. (2005) 'Aligning fast alternating current electroosmotic flow fields and characteristic frequencies with dielectrophoretic traps to achieve rapid bacteria detection' *Electrophoresis*, **26**, 3725–3737.

Gagnon, Z., Senapati, S., Gordon, J. and Chang H.-C. (2009) 'Dielectrophoretic detection and quantification of hybridized DNA molecules on nano-genetic particles' *Electrophoresis* **29**, 4808–4812.

Gervais, L. and Delamarche, E. (2009) 'Toward one-step point-of-care immunodiagnostics using capillary-driven microfluidics and PDMS substrates' *Lab Chip*, **9**, 3330–3337.

Glass, N. R., Shilton, R. J., Chan, P. P. Y., Friend, J. R. and Yeo, L. Y. (2012) 'Miniaturized Lab-on-a-Disc (miniLOAD)' *Small*, **8**, 1881–1888.

González, A., Ramos, A., Green, N. G., Castellanos, A. and Morgan H. (2000) 'Fluid flow induced by nonuniform ac electric fields in electrolytes on microelectrodes. II. A linear double-layer analysis' *Phys. Rev. E*, **61**, 4019–4028.

Gorkin, III R. Clime, L. Madou, M. and Kido, H. (2010) 'Pneumatic pumping in centrifugal microfluidic platforms' *Microfluid. Nanofluid.*, **9**, 541–549.

Green, N. G. and Morgan, H. (1999) 'Dielectrophoresis of submicrometer latex spheres. 1. Experimental results' *J. Phys. Chem. B*, **103**, 41–50.

Grier, D. G. (1997) 'Optical tweezers in colloid and interface science' *Curr. Op. Colloid Interface Sci.*, **2**, 264–270.

Grigoriev, R. O. (2005) 'Optical tweezers in colloid and interface science' *Phys. Fluids*, **17**, 033601.

Grover, W. H., Ivester, R. H. C., Jensen, E. C. and Mathies, R. A. (2006) 'Development and multiplexed control of latching pneumatic valves using microfluidic logical structures' *Lab Chip*, **6**, 623–631.

Harris, N. R, Hill, M., Townsend, R., White, N. M. and. Beeby S. P. (2005) 'Performance of a micro-engineered ultrasonic particle manipulator' *Sens. Actuators B: Chemical*, **111**, 481–486.

Hart, S. J. and Terray, A. V. (2003) 'Refractive-index-driven separation of colloidal polymer particles using optical chromatography' *Appl. Phys. Lett.*, **83**, 5316–5318.

Hart, S. J., Terray, A., Arnold, J. and Leski, T. A. (2007) 'Sample concentration using optical chromatography' *Opt. Express*, **15**, 2724–2731.

Hashmi, A., Yua, G., Reilly-Collette, M., Heiman, G. and Xu, J. (2012) 'Oscillating bubbles: a versatile tool for lab on a chip applications' *Lab Chip*, **12**, 4216–4227, DOI: 10.1039/C2LC40424A.

Hawkes, J. J. and Coakley, W. T. (2001) 'Force field particle filter, combining ultrasound standing waves and laminar flow' *Sens. Actuat. B: Chem.*, **75**, 213–222.

Heron, S. R., Wilson, R., Shaffer, S. A., Goodlett, D. R. and Cooper, J. M. (2010) 'Surface acoustic wave nebulization of peptides as a microfluidic interface for mass spectrometry' *Anal. Chem.*, **82**, 3985–3989.

Herr, A. E., Molho, J. I., Santiago, J. G., Mungal, M. G., Kenny, T. W. and Garguilo, M. G. (2000) 'Electroosmotic capillary flow with nonuniform zeta potential' *Anal. Chem.*, **72**, 1053–1057.

Ho, J., Tan, M. K., Go, D., Yeo, L. Y., Friend, J. R. and Chang, H.-C. (2011) 'A paper-based microfluidic surface acoustic wave sample delivery and ionization source for rapid and sensitive ambient mass spectrometry' *Anal. Chem.*, **83**, 3260–3266.

Hodgson, R. P., Tan, M., Yeo, L. Y. and Friend, J. R. (2009) 'Transmitting high power RF acoustic radiation via fluid couplants into superstrates for microfluidics' *Appl. Phys. Lett.*, **94**, 024102.

Hunter, R. J. (1987) *Foundations of Colloid Science*, Vol. 1 (Oxford University, Oxford).

Ichikawa, N., Hosokawa, K. and Maeda, R. (2004) 'Interface motion of capillary-driven flow in rectangular microchannel' *J. Colloid Interface Sci.*, **280**, 155–164.

Jang, J. and Lee, S. S. (2000) 'Theoretical and experimental study of MHD (magneto-hydrodynamic) micropump' *Sens. Actuators A: Phys.*, **80**, 84–85.

Jang, L. S., Li Y. J., Lin S. J., Hsu, Y. C., Yao, W. S., Tsai, M. C. and Hou, C. C. (2007) 'A stand-alone peristaltic micropump based on piezoelectric actuation' *Biomed. Microdev.*, **9**, 185–194.

Jeong, O. K. and Yang, S. S. (2000) 'Fabrication and test of a thermopneumatic micropump with a corrugated $p+$ diaphragm' *Sens. Actuators A: Physical*, **83**, 249–255.

Johansson, L., Enlund, J., Johansson, S., Katardjiev, I., Wiklund, M. and Yantchev, V. (2012) 'Surface acoustic wave-induced precise particle manipulation in a trapezoidal glass microfluidic channel' *J. Micromech. Microeng.*, **22**, 025018.

Johnson, D. A. and Feke D. L. (1995) 'Methodology for fractionating suspended particles using ultrasonic standing wave and divided flow fields' *Sep. Tech.*, **5**, 251–258.

Kenyon, S. M., Meighan, M. M. and Haye, M. A., (2011) 'Recent developments in electrophoretic separations on microfluidic devices' *Electrophoresis*, **32**, 482–93.

Kim, J.-H, Na, K.-H., Kang, C. J. and Kim, Y.-S. (2005) 'A disposable thermopneumatic-actuated micropump stacked with PDMS layers and ITO-coated glass' *Sens Actuators A: Physical*, **120**, 365–369.

Koch, M., Harris, N., Evans, A. G. R., White, N. M. and Brunnschweiler, A. (1998) 'A novel micromachined pump based on thick-film piezoelectric actuation' *Sens. Actuators A*, **70**, 98–103.

Kulkarni, K. P., Friend, J. R., Yeo, L. Y. and Perlmutter, P. (2009) 'Surface acoustic waves as an energy source for drop scale synthetic chemistry' *Lab Chip*, **9**, 754–755.

Kulkarni, K. P., Ramarathinam, S. H., Friend, J. R., Yeo, L. Y., Purcell, A. W. and Perlmutter, P. (2010) 'Rapid microscale in-gel processing and digestion of proteins using surface acoustic waves' *Lab Chip*, **10**, 1518–1520.

Langelier, S. M., Yeo, L. Y. and Friend, J. R. (2012) 'UV epoxy bonding for enhanced SAW transmission and microscale acoustofluidic integration' *Lab Chip*, **12**, 2970–2976.

Lastochkin, D., Zhou, R., Wang, P., Ben, Y. and Chang, H.-C. (2004) 'Electrokinetic micropump and micromixer design based on ac Faradaic polarisation' *J. Appl. Phys.*, **96**, 1730–1733.

Laurell, T., Petersson, F. and Nilsson A. (2007) 'Chip integrated strategies for acoustic separation and manipulation of cells and particles' *Chem. Soc. Rev.*, **36**, 492–506.

Lazar, I. M. and Karger, B. L. (2002) 'Multiple open-channel electroosmotic pumping system for microfluidic sample handling' *Anal. Chem.*, **74**, 6259–6268.

Lemoff, A. V. and Lee, A. P. (2000) 'An AC magnetohydrodynamic micropump' *Sens. Actuators B: Chemical*, **63**,178–185.

Li, H., Friend, J. R. and Yeo, L. Y. (2007b) 'Surface acoustic wave concentration of particle and bioparticle suspensions' *Biomed. Microdev.*, **9**, 647–656.

Li, H., Friend, J. R. and Yeo, L. Y. (2008) 'Microfluidic colloidal island formation and erasure induced by surface acoustic wave radiation' *Phys. Rev. Lett.*, **101**, 084502.

Li, H., Friend, J. R. and Yeo, L. Y. (2007a) 'A scaffold cell seeding method driven by surface acoustic waves' *Biomaterials*, **28**, 4098–4104.

Li, Y., Fu, Y. Q., Brodie, S. D., Alghane, M. and Walton A. J. (2012) 'Integrated microfluidics system using surface acoustic wave and electrowetting on dielectrics technology' *Biomicrofluidics*, **6**, 012812.

Lighthill, J. (1978) 'Acoustic streaming' *J. Sound Vib.*, **61**, 391–418.

Lin, H.-Y., Tsai, L.-C., Chi, P.-Y. and Chen, C.-D. (2005) 'Positioning of extended individual DNA molecules on electrodes by non-uniform AC electric fields' *Nanotechnology*, **16**, 2738–2742.

Lin, H., Storey, B. D., Oddy, M. H., Chen, C.-H. and Santiago, J. G. (2004) 'Instability of electrokinetic microchannel flows with conductivity gradients' *Phys. Fluids*, **16**, 1922–1935.

Lin, S. C., Mao, X. and Huang T. J. (2012) 'Surface acoustic wave (SAW) acoustophoresis: now and beyond' *Lab Chip*, **12**, 2766–2770.

Liu, Y. and Lim, K. M. (2011) 'Particle separation in microfluidics using a switching ultrasonic field' *Lab Chip*, **11**, 3167–3173.

Luginbuhl, P., Collins, S. D., Racine, G., Gretillat, M. A., Rooij, N. F. D., Brooks, K. G. and Setter, N. (1997) 'Microfabricated lamb wave device based on PZT Sol–gel thin film for mechanical transport of solid particles and liquids' *J. Microelectromech. Sys.*, **6**, 337–345.

Machauf, A., Nemirovsky, Y. and Dinnar, U. (2005) 'A membrane micropump electrostatically actuated across the working fluid' *J. Micromech. Microeng.*, **15**, 2309–2316.

Madou, M., Zoval, J., Jia, G., Kido, H., Kim, J. and Kim, N. (2006) 'Lab on a CD' *Annu. Rev. Biomed. Eng.*, **8**, 601–628.

Manneberg, O., Hagsäter, M. S., Svennebring, J., Hertz H. M., Kutter J. P., Bruus, H. and Wiklund, M. (2009) 'Spatial confinement of ultrasonic force fields in microfluidic channels' *Ultrasonics*, **49**, 112–119.

Manor, O., Dentry, M., Friend, J. R. and Yeo, L. Y. (2011) 'Substrate dependent drop deformation and wetting under high frequency vibration' *Soft Matter*, **7**, 7976–7979.

Manor, Yeo, L. Y. and Friend, J. R. (2012) 'The appearance of boundary layers and drift flows due to high-frequency surface waves' *J. Fluid Mech.*, **707**, 482–495.

Martinez, A. W., Phillips, S. T. and Whitesides, G. M. (2010) 'Diagnostics for the developing world: microfluidic paper-based analytical devices' *Anal. Chem.*, **82**, 3–10.

Masini, L., Cecchini, M., Girardo, S., Cingolani, R., Pisignano, D. and Beltram, F. (2010) 'Surface-acoustic-wave counterflow micropumps for on-chip liquid motion control in two-dimensional microchannel arrays' *Lab Chip*, **10**, 1997–2000.

Meagher, R. J., Won, J. I., McCormick, L. C., Nedelcu, S., Bertrand, M. M., Bertram, J. L., Drouin, G., Barron, A. E. and Slater, G. W. (2005) 'End-labeled free-solution electrophoresis of DNA' *Electrophoresis*, **26**, 331–50.

Menachery, A., Graham D., Messerli, S. M., and Pethig, R. and Smith, P. J. S. (2011) 'Dielectrophoretic tweezer for isolating and manipulating target cells' *IET Nanobiotechnol.*, **5**,1–7.

Meng, A. H., Nguyen, N.-T. and White, R. M. (2000) 'Focused flow micropump using ultrasonic flexural plate waves' *Biomed. Microdev.*, **2**, 169–174.

Meng, L., Cai, F., Zhang, Z., Niu, L., Jin, Q., Yan, F., Wu, J., Wang, Z. and Zheng, H. (2011) 'Transportation of single cell and microbubbles by phase-shift introduced to standing leaky surface acoustic waves' *Biomicrofluidics*, **5**, 044104.

Minerick, A. R., Ostafin A. E. and Chang, H.-C. (2002) 'Electrokinetic transport of red blood cells in microcapillaries' *Electrophoresis*, **23**, 2165–2173.

Moroney, R. M., White, R. M. and Howe R. T. (1991) 'Microtransport induced by ultrasonic Lamb waves' *Appl. Phys. Lett.*, **59**, 774–776.

Mugele, F. and Baret, J.-C. (2005) 'Electrowetting: from basics to applications' *J. Phys.: Condens. Matter*, **17**, R705–R774.

Mukhopadhyay, R. (2006) 'What does nanofluidics have to offer?' *Anal. Chem.*, **78**, 7379–7382.

Nam, J., Lim, H., Kim, C., Kang, J. Y. and Shin, S. (2012) 'Density-dependent separation of encapsulated cells in a microfluidic channel by using a standing surface acoustic wave' *Biomicrofluidics*, **6**, 024120.

Napoli, M., Eijkel, J. C. and Pennathur, S. (2010) 'Nanofluidic technology for biomolecule applications: a critical review' *Lab Chip*, **10**, 957–85.

Natraj, V. and Chen, S. B. (2002) 'Primary electroviscous effect in a suspension of charged porous spheres' *J. Colloid Interface Sci.*, **251**, 200–207.

Neale, S. L., Macdonald, M. P., Dholakia, K., and Krauss, T. F. (2005) 'All-optical control of microfluidic components using form birefringence' *Nat. Mater.*, **4**, 53–533.

Ng, W. Y., Lam Y. C. and Rodríguez, I. (2009) 'Experimental verification of Faradaic charging in ac electrokinetics' *Biomicrofluidics*, **3**, 022405.

Noblin, X., Buguin, A. and Brochard-Wyart, F. (2004) 'Vibrated sessile drops: transition between pinned and mobile contact line oscillations' *Eur. Phys. J. E*, **14**, 395–404.

Nyborg, W. L. (1958) 'Acoustic streaming near a boundary' *J. Acoust. Soc. Am.*, **30**, 329–339.

Ohl, C.-D., Arora, M., Ikink, R., Jong, N. D. Versluis, M., Delius, M. and Lohse, D. (2006) 'Sonoporation from jetting cavitation bubbles' *Biophys. J.*, **91**, 4285–4295.

Orloff, N. D., Dennis, J. R., Cecchini, M., Schonbrun, E., Rocas, E., Wang, Y., Novotny, D., Simmonds, R. W., Moreland, J., Takeuchi, I. and Booth, J. C. (2011) 'Manipulating particle trajectories with phase-control in surface acoustic wave microfluidics' *Biomicrofluidics*, **5**, 044107.

Paegel B. M., Emrich, C. A., Wedemayer, G. J., Scherer, J. R. and Mathies, R. A. (2002) 'High throughput DNA sequencing with a microfabricated 96-lane capillary array electrophoresis bioprocessor' *Proc. Natl. Acad. Sci. USA*, **99**, 574–579.

Pan, Y.-J., Ren, C.-M. and Yang, R.-J. (2007) 'Electrokinetic flow focusing and valveless switching integrated with electrokinetic instability for mixing enhancement' *J. Micromech. Microeng.*, **17**, 820–827.

Patel, M. V.,Tovar, A. R. and Lee, A. P. (2012) 'Lateral cavity acoustic transducer as an on-chip cell/particle microfluidic switch' *Lab Chip*, **12**, 139–145.

Petersson, F., Nilsson, A., Holm, C., Jönsson, H. and Laurell, T. (2004) 'Separation of lipids from blood utilizing ultrasonic standing waves in microfluidic channels' *Analyst*, **129**, 938–943.

Pethig, R. (2010) 'Dielectrophoresis: status of the theory, technology, and applications' *Biomicrofluidics*, **4**, 022811.

Petsev, D. N. (2010) 'Transport in fluidic nanochannels' *Surfactant Sci. Ser.*, **147**, 221–247.

Piruska, A., Gong, M., Sweedler, J. V. and Bohn, P. W. (2010) 'Nanofluidics in chemical analysis' *Chem. Soc. Rev.*, **39**, 1060–1072.

Pol, F. C. M., Lintel, H. T. G., Elwenspoek, M. and Fluitman, J. H. J. (1990) 'A thermopneumatic micropump based on micro-engineering techniques' *Sens. Actuators A: Physical*, **21**, 198–202.

Qi, A., Chan, P., Ho, J., Rajapaksa, A., Friend, J. R. and Yeo, L. Y. (2011) 'Template-free synthesis and encapsulation technique for layer-by-layer polymer nanocarrier fabrication' *ACS Nano*, **5**, 9583–9591.

Qi, A., Friend, J.R., Yeo, L. Y., Morton, D.A., McIntosh, M. P. and Spiccia, L. (2009) 'Miniature inhalation therapy platform using surface acoustic wave microfluidic atomization' *Lab Chip*, **9**, 2184–2193.

Qi, A., Yeo, L. Y. and Friend J. R. (2008) 'Interfacial destabilization and atomization driven by surface acoustic waves' *Phys. Fluids*, **20**, 074103.

Qi, A., Yeo. L. Y., Friend, J. R. and Ho, J. (2010) 'The extraction of liquid, protein molecules and yeast cells from paper through surface acoustic wave atomization' *Lab Chip*, **10**, 470–476.

Qiao, R. and Aluru, N. R. (2003) 'Ion concentrations and velocity profiles in nanochannel electroosmotic flows' *J. Chem. Phys.*, **118**, 4692–4701.

Ramos, A., González, A., Castellanos, A., Green, N. G. and Morgan, H. (2003) 'Pumping of liquids with ac voltages applied to asymmetric pairs of microelectrodes' *Phys. Rev. E*, **67**, 0563.

Rauscher, M. and Dietrich, S. (2008) 'Wetting phenomena in nanofluidics' *Annu. Rev. Mater. Res.*, **38**, 143–172.

Rayleigh, L. (1884) 'On the circulation of air observed in Kundt's tubes and on some allied acoustical problems' *Phil. Trans. R. Soc. Lond.*, **175**, 1–21.

Renaudin, A., Tabourier, P., Zhang, V., Camart, J. C. and Druon, C. (2006) 'SAW nanopump for handling droplets in view of biological applications' *Sens. Actuators B: Chemical*, **113**, 389–397.

Rezk, A. R., Manor, O., Friend, J. R. and Yeo, L. Y. (2012a) 'Acoustowetting: film spreading, fingering instabilities and soliton-like wave propagation', *Nat. Commun.*, **3**, 1167.

Rezk, A. R., Qi, A., Friend, J. R., Li, W. H. and Yeo, L. Y. (2012b) 'Uniform mixing in paper-based microfluidic systems using surface acoustic waves' *Lab Chip*, 12, 773–779.

Robinson, T. and Dittrich, P. S. (2013) 'Microfluidic technology for molecular diagnostics' *Adv. Biochem. Eng. Biotechnol.*, **133**, 89–114, DOI: 10.1007/10_2012_139.

Rogers, P. R., Friend, J. R. and Yeo, L. Y. (2010) 'Exploitation of surface acoustic waves to drive size-dependent microparticle concentration within a droplet' *Lab Chip*, **10**, 2979–2985.

Schabmueller, C. G. J., Koch, M., Mokhtari, M. E., Evans, A. G. R., Brunnschweiler, A. and Sehr, H. (2002) 'Self-aligning gas/liquid micropump' *J. Micromech. Microeng.*, **12**, 420–424.

Schlichting, H. (1932) 'Calculation of even periodic barrier currents' *Physik. Z.*, **33**, 327–335.

Schmid, L., Wixforth, A., Weitz, D. A. and Franke, T. (2012) 'Novel surface acoustic wave (SAW)-driven closed PDMS flow chamber' *Microfluid. Nanofluid.*, **12**, 229–235.

Schneider, S. W., Nuschele, S., Wixforth, A., Gorzelanny, C., Alexander-Katz, A., Netz, R. R. and Schneider, M. F. (2007) 'Shear-induced unfolding triggers adhesion of von Willebrand factor fibers' *Proc. Natl. Acad. Sci. USA*, **104**, 7899–7903.

Schoch, R. B., Han, J. and Renaud, P. (2008) 'Transport phenomena in nanofluidics' *Rev. Mod. Phys.*, **80**, 839–883.

Shi, J., Ahmed, D., Mao, X., Lin, S. C. S., Lawit, A. and Huang, T. J. (2009) 'Acoustic tweezers: patterning cells and microparticles using standing surface acoustic waves (SSAW)' *Lab. Chip*, **9**, 2890–2895.

Shi, J., Mao, X., Ahmed, D., Colletti, A. and Huang, T. J. (2008) 'Focusing microparticles in a microfluidic channel with standing surface acoustic waves (SSAW)' *Lab Chip*, **8**, 221–223.

Shilton, R. J., Yeo, L. Y. and Friend, J. R. (2011) 'Quantification of surface acoustic wave induced chaotic mixing-flows in microfluidic wells' *Sens. Actuators B: Chemical*, **160**, 1565–1572.

Shilton, R., Tan M. K., Yeo, L. Y. and Friend, J. R. (2008) 'Particle concentration and mixing in microdrops driven by focused surface acoustic waves' *J. Appl. Phys.*, **104**, 014910.

Shubin, V. E., Hunter, R. J. and O'Brien, R. W. (1993) 'Electroacoustic and dielectric study of surface conduction' *J. Colloid Interface Sci.*, **159**, 174–183.

Sparreboom, W., van den Berg, A. and. Eijkel, J. C. T. (2009) 'Principles and applications of nanofluidic transport' *Nat. Nanotechnol.*, **4**, 713–720.

Squires, T. M. and Bazant, M. A. (2004) 'Induced-charge electro-osmosis' *J. Fluid Mech.*, **509**, 217–252.

Squires, T. M. and Quake, S. R. (2005) 'Microfluidics: fluid physics at the nanoliter scale' *Rev. Mod. Phys.*, **77**, 977–1026.

Stern, O. (1924) 'The theory of electrical double layer' *Z. Elektrochem.*, **30**, 508–516.

Suzuki, H. and Yoneyama, R. (2002) 'A reversible electrochemical nanosyringe pump and some considerations to realize low power consumption' *Sens. Actuators B*, **86**, 242–250.

Szántai, E. and Guttman, A. (2006) 'Genotyping with microfluidic devices' *Electrophoresis*, **27**, 4896–4903.

Takamura, Y., Onoda, H., Inokuchi, H., Adachi, S., Oki, A. and Horiike, Y. (2003) 'Low-voltage electroosmosis pump for stand-alone microfluidics devices' *Electrophoresis*, **24**, 185–192.

Tan, M. K., Friend, J. R. and Yeo, L. Y. (2007) 'Microparticle collection and concentration via a miniature surface acoustic wave device' *Lab Chip*, **7**, 618–625.

Tan, M. K., Yeo, L. Y. and Friend, J. R. (2009b) 'Interfacial jetting phenomena induced by focused surface vibrations' *Phys. Rev. Lett.*, **103**, 024501.

Tan, M. K., Yeo, L. Y. and Friend, J. R. (2010) 'Unique flow transitions and particle collection switching phenomena in a microchannel induced by surface acoustic waves' *Appl. Phys. Lett.*, **97**, 234106.

Tan, M. K., Yeo, L. Y. and Friend, J. R. (2009a) 'Rapid fluid flow and mixing induced in microchannels using surface acoustic waves' *Europhys. Lett.*, **87**, 47003.

Tovar, A. R. and Lee, A. P. (2009) 'Lateral cavity acoustic transducer' *Lab Chip*, **9**, 41–43.

Vyawahare, S., Sitaula, S., Martin, S., Adalianb, D. and Scherer, A. (2008) 'Electronic control of elastomeric microfluidic circuits with shape memory actuators' *Lab Chip*, **8**, 1530–1535.

Wang, C., Jalikop, S. V. and Hilgenfeldt, S. (2012) 'Efficient manipulation of microparticles in bubble streaming flows' *Biomicrofluidics*, **6**, 012801.

Wang, P., Chen, Z. and Chang, H.-C. (2006) 'A new electro-osmotic pump based on silica monoliths' *Sens. Actuators B: Chemical*, **113**, 500–509.

Wang, X., Wang, S., Gendhar, B., Cheng, C., Byun, C. K., Li, G, Zhao, M. and Liu, S. (2009) 'Electroosmotic pumps for microflow analysis' *Trends Anal. Chem.*, **28**, 64–74.

Wheeler, A. R. (2008) 'Putting electrowetting to work' *Science*, **322**, 539–540.

Wixforth, A., Strobl, C., Gauer, C. H., Toegl, A., Scriba, J. and Guttenberg, Z. V. (2004) 'Acoustic manipulation of small droplets' *Anal. Bioanal. Chem.*, **379**, 982–991.

Wu, D., Qin, J. and Lin, B. (2008) 'Electrophoretic separations on microfluidic chips' *J. Chromatogr. A*, **1184**, 542–559.

Xu, D., Wang, L., Ding, G., Zhou, Y., Yu, A. and Cai, B. (2001) 'Characteristics and fabrication of NiTi/Si diaphragm micropump' *Sens. Actuators A: Physical*, **93**, 87–92.

Yaralioglu, G. G., Wygant, I. O., Marentis, T. C. and Khuri-Yakub, B. T. (2004) 'Ultrasonic mixing in microfluidic channels using integrated transducers' *Anal. Chem.*, **76**, 3694–3698.

Yeo, L. Y. and Chang, H.-C. (2005) 'Static and spontaneous electrowetting' *Mod. Phys. Lett. B*, **19**, 549–569.

Yeo, L. Y., Chang, H.-C., Chan, P. P. Y. and Friend, J. R. (2011) 'Microfluidic devices for bioapplications' *Small*, **7**, 12–48.

Yeo, L.Y. and Friend, J. R. (2009). 'Ultrafast microfluidics using surface acoustic waves', *Biomicrofluidics* **3**, 012002.

Yin, Z. and Prosperetti, A. (2005) 'A microfluidic 'blinking bubble' pump' *J. Micromech. Microeng.*, **15**, 643–651.

Yoshimi, Y., Shinoda, K., Mishima, M., Nakao, K. and Munekane, K. (2004) 'Development of an artificial synapse using an electrochemical micropump' *J. Artif. Organs*, **7**, 210–215.

Zhou, Y. and Amirouche, F. (2011) 'An electromagnetically-actuated all-PDMS valveless micropump for drug delivery' *Micromachines*, **2**, 345–355.

Zhou, K., Perry, J. M. and Jacobson, S. C. (2011). 'Transport and sensing in nanofluidic devices' *Annu. Rev. Anal. Chem.*, **4**, 321–341.